

AD-A089 410

RENSSELAER POLYTECHNIC INST TROY NY DEPT OF ELECTRIC--ETC F/6 9/1  
RADIATION EFFECTS ON THE MICROWAVE PROPERTIES OF SAAS MESFETS.(U)  
JUN 80 J M BORREGO, R J GUTMANN, S B MOGHE F19628-78-C-0097

UNCLASSIFIED

RADC-TR-80-171

NL

[ 04 ]  
45 A  
095010



END

DATE

FILED

10-80

DTIC

AD A089410

**RADC-TR-80-171**  
Final Technical Report  
June 1980



# **RADIATION EFFECTS ON THE MICROWAVE PROPERTIES OF GaAs MESFETs**

**Rensselaer Polytechnic Institute**

Jose M. Borrego  
Ronald J. Gutmann  
Sanjay B. Moghe  
Kevin G. Rochford

APPROVED FOR PUBLIC RELEASE; DISTRIBUTION UNLIMITED

**DTIC**  
**ELECT**  
**SEP 23 1980**  
**B**

**ROME AIR DEVELOPMENT CENTER**  
**Air Force Systems Command**  
**Griffiss Air Force Base, New York 13441**

DOC FILE COPY

80 9 22 005

This report has been reviewed by the RADC Public Affairs Office (PAO) and is releasable to the National Technical Information Service (NTIS). At NTIS it will be releasable to the general public, including foreign nations.

RADC-TR-80-171 has been reviewed and is approved for publication.

APPROVED:

*Henry M. DeAngelis*

HENRY M. DEANGELIS  
Project Engineer

APPROVED:

*Clarence D. Turner*

CLARENCE D. TURNER, Acting Director  
Solid State Sciences Division

FOR THE COMMANDER:

*John P. Huss*

JOHN P. HUSS  
Acting Chief, Plans Office

If your address has changed or if you wish to be removed from the RADC mailing list, or if the addressee is no longer employed by your organization, please notify RADC (ESR), Hanscom AFB MA 01731. This will assist us in maintaining a current mailing list.

Do not return this copy. Retain or destroy.

UNCLASSIFIED

SECURITY CLASSIFICATION OF THIS PAGE (When Data Entered)

19 REPORT DOCUMENTATION PAGE		READ INSTRUCTIONS BEFORE COMPLETING FORM
18 1. REPORT NUMBER RADCTR-80-171	2. GOVT ACCESSION NO. AD A089410	3. RECIPIENT'S CATALOG NUMBER
6 4. TITLE (and Subtitle) RADIATION EFFECTS ON THE MICROWAVE PROPERTIES OF GaAs MESFETS	9 5. TYPE OF REPORT & PERIOD COVERED Final Technical Report. 1 Apr 78 - 30 Jun 79	6. PERFORMING ORG. REPORT NUMBER N/A
10 7. AUTHOR(s) Jose M. / Borrego Ronald J. / Gutmann	15 8. CONTRACT OR GRANT NUMBER(s) F19628-78-C-0097	
9. PERFORMING ORGANIZATION NAME AND ADDRESS Rensselaer Polytechnic Institute Electrical and Systems Engineering Department Troy NY 12181		10. PROGRAM ELEMENT, PROJECT, TASK AREA & WORK UNIT NUMBERS 61102F 23060327
11. CONTROLLING OFFICE NAME AND ADDRESS Deputy for Electronic Technology (RADC/ESR) Hanscom AFB MA 01731		17 J3
14. MONITORING AGENCY NAME & ADDRESS (if different from Controlling Office) Same		12 71
16. DISTRIBUTION STATEMENT (of this Report) Approved for public release; distribution unlimited.		15. SECURITY CLASS. (of this report) UNCLASSIFIED
17. DISTRIBUTION STATEMENT (of the abstract entered in Block 20, if different from Report) Same		15a. DECLASSIFICATION/DOWNGRADING SCHEDULE N/A
18. SUPPLEMENTARY NOTES RADC Project Engineer: Henry M. DeAngelis (RADC/ESR)		
19. KEY WORDS (Continue on reverse side if necessary and identify by block number) GaAs MESFET Newtron Radiation Effects Gamma Radiation Effects Microwave Amplifier Noise Schottky Gate		
20. ABSTRACT (Continue on reverse side if necessary and identify by block number) The effect of fast neutron and gamma irradiation on the electrical characteristics of low noise microwave GaAs MESFET amplifiers has been evaluated. The microwave amplifiers were realized on alumina microstrip using commercial devices mounted in a common source configuration. The changes in the noise figure and amplifier gain at S- and X-band were determined for neutron fluences between $3 \times 10^{12}$ to $1 \times 10^{15}$ n/cm <sup>2</sup> and for a gamma dose of $2 \times 10^7$ rads (Si). Continued		

DD FORM 1473

EDITION OF 1 NOV 65 IS OBSOLETE

UNCLASSIFIED

SECURITY CLASSIFICATION OF THIS PAGE (When Data Entered)

10 to the 7th power

401653

gsm

UNCLASSIFIED

SECURITY CLASSIFICATION OF THIS PAGE(When Data Entered)

Item 20 (Cont'd)

The noise figure starts to be affected at  $1 \times 10^{14}$  n/cm<sup>2</sup> and a large deterioration is observed at  $1 \times 10^{15}$  n/cm<sup>2</sup>. The increase in noise figure is related to the decrease in transconductance and increase in the parasitic source resistance. The decrease in the amplifier gain at the high neutron fluence is due to a deterioration of the transconductance, source resistance and change in the gate to source and gate to drain capacitances. The low frequency noise increases with neutron radiation but not with  $\gamma$ -radiation. The low frequency noise appears not to be correlated with the microwave noise. Gamma irradiation increases the noise figure at a dose of  $2 \times 10^7$  rads (Si) without affecting the signal characteristics of the device. It appears that  $\gamma$ -radiation produces levels which respond at microwave frequencies.

10 to the 15th power

10 to the 14th power  
pg. cm

10 to the 7th power

gamma

GAU4



UNCLASSIFIED

SECURITY CLASSIFICATION OF THIS PAGE(When Data Entered)

# TABLE OF CONTENTS

	<u>Page</u>
LIST OF FIGURES . . . . .	iv
LIST OF TABLES . . . . .	vii
FOREWORD . . . . .	viii
1. INTRODUCTION . . . . .	1
1.1 Introduction . . . . .	1
1.2 Program Outline . . . . .	2
2. AMPLIFIERS TESTED AND MEASUREMENT PROCEDURES . . . . .	4
2.1 Device Tested . . . . .	4
2.2 Low Frequency Measurements . . . . .	9
2.3 Microwave Measurements . . . . .	11
2.4 Radiation Testing . . . . .	15
3. RESULTS AND DISCUSSION . . . . .	19
3.1 Introduction . . . . .	19
3.2 Low Neutron Fluence Results . . . . .	19
3.3 Changes in Low Frequency Characteristics at High Neutron Neutron Fluences . . . . .	22
3.4 Changes in Microwave Noise and Gain at High Neutron Fluences . . . . .	26
3.5 $\gamma$ -Radiation Results . . . . .	51
4. CONCLUSIONS . . . . .	57
5. BIBLIOGRAPHY . . . . .	59

ACCESSION for		
NTIS	White Section	<input checked="" type="checkbox"/>
DDC	Buff Section	<input type="checkbox"/>
UNANNOUNCED		<input type="checkbox"/>
JUSTIFICATION		
BY		
DISTRIBUTION/AVAILABILITY CODES		
Dist.	AVAIL. and/or	SPECIAL
A		

# LIST OF FIGURES

	<u>Page</u>
Fig. 2.1 Chip Mounting Disc . . . . .	5
Fig. 2.2 Microstrip Device-Testing Structure . . . . .	5
Fig. 2.3 GaAs FET Chip on Disc Showing Bonding Wires (chip dimensions 0.025" x 0.011" x 0.005") . . . . .	6
Fig. 2.4 S-Band Amplifier with Tuning Discs . . . . .	8
Fig. 2.5 X-Band Amplifier with Tuning Discs and Protective Cap over Chip . . . . .	8
Fig. 2.6 Schematic of Low-frequency Test Set-up . . . . .	10
Fig. 2.7 Schematic Diagram of S-Band Amplifier Noise and Gain Measurement Set-up . . . . .	12
Fig. 2.8 X-Band Amplifier (Gain and Noise Figure) and Device (Scattering Parameter) Measurement Set-up . . . . .	14
Fig. 2.9 Schematic Diagram of S-Band Scattering Parameter Measure- ment Set-up . . . . .	16
Fig. 3.1 Change in the Drain Current vs. Drain Voltage DC Characteristics at Low Neutron Fluences . . . . .	20
Fig. 3.2 Change in the Low Frequency Equivalent Noise Input Voltage . . . . .	21
Fig. 3.3 Drain Current vs. Drain Voltage DC Characteristics after High Neutron Fluences . . . . .	23
Fig. 3.4 Drain Current vs. Drain Voltage DC Characteristics after High Neutron Fluences . . . . .	24
Fig. 3.5 Drain Current vs. Drain Voltage DC Characteristics after High Neutron Fluences . . . . .	25
Fig. 3.6 1 MHz Transconductance vs. Gate Voltage Characteristics after High Neutron Fluence . . . . .	27
Fig. 3.7 1 MHz Transconductance vs. Gate Voltage Characteristics after High Neutron Fluence . . . . .	28
Fig. 3.8 1 MHz Transconductance vs. Gate Voltage Characteristics after High Neutron Fluence . . . . .	29

LIST OF FIGURES cont.

	<u>Page</u>
Fig. 3.9 Low Frequency Equivalent Noise Input Voltage as a Function of Frequency after High Neutron Fluence . . .	30
Fig. 3.10 Low Frequency Equivalent Noise Input Voltage as a Function of Frequency after High Neutron Fluence . . .	31
Fig. 3.11 Low Frequency Equivalent Noise Input Voltage as a Function of Frequency after High Neutron Fluence . . .	32
Fig. 3.12 Change in the Noise Figure vs. Gate Voltage Characteristics at 3 GHz after High Neutron Fluence . . . .	33
Fig. 3.13 Change in the Noise Figure vs. Gate Voltage Characteristics at 3 GHz after High Neutron Fluence . . . .	34
Fig. 3.14 Change in the Noise Figure vs. Gate Voltage Characteristics at 3 GHz after High Neutron Fluence . . . .	35
Fig. 3.15 Change in the Amplifier Gain vs. Gate Voltage Characteristics at 3 GHz after High Neutron Fluence . . . .	36
Fig. 3.16 Change in the Amplifier Gain vs. Gate Voltage Characteristics at 3 GHz after High Neutron Fluence . . . .	37
Fig. 3.17 Change in the Amplifier Gain vs. Gate Voltage Characteristics at 3 GHz after High Neutron Fluence . . . .	38
Fig. 3.18 Noise Figure vs. Gate Voltage at X-Band after High Neutron Fluence . . . . .	40
Fig. 3.19 Noise Figure vs. Gate Voltage at X-Band after High Neutron Fluence . . . . .	41
Fig. 3.20 Noise Figure vs. Gate Voltage at X-Band after High Neutron Fluence . . . . .	42
Fig. 3.21 Amplifier Gain vs. Gate Voltage at X-Band after High Neutron Fluence . . . . .	43
Fig. 3.22 Amplifier Gain vs. Gate Voltage at X-Band after High Neutron Fluence . . . . .	44
Fig. 3.23 Amplifier Gain vs. Gate Voltage at X-Band after High Neutron Fluence . . . . .	45
Fig. 3.24 Drain to Source Resistance as a Function of Normalized Gate Voltage . . . . .	49



LIST OF FIGURES cont.

	<u>Page</u>
Fig. 3.25 Measured and Predicted Noise Figure vs. Gate Voltage after $1 \times 10^{15}$ n/cm <sup>2</sup> . . . . .	50
Fig. 3.26 Measured and Predicted Noise Figure vs. Gate Voltage after $1 \times 10^{15}$ n/cm <sup>2</sup> . . . . .	52
Fig. 3.27 Measured and Predicted Noise Figure vs. Gate Voltage after $1 \times 10^{15}$ n/cm <sup>2</sup> . . . . .	53
Fig. 3.28 $\gamma$ -Irradiated Amplifier Characteristics vs. Gate Voltage at 3 GHz . . . . .	54
Fig. 3.29 $\gamma$ -Irradiated Amplifier Characteristics vs. Gate Voltage at 10 GHz . . . . .	55

## LIST OF TABLES

	<u>Page</u>
Table 2.1 Radiation Summary . . . . .	18
Table 3.1 Amplifier Characteristics Before and After Neutron Irradiation with Pre-Irradiation Minimum Noise Figure Bias . . . . .	47

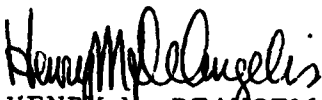
## PREFACE

Under RADC, Deputy for Electronic Technology, Contract No. F19628-78-C-0097, the Electrical and Systems Engineering Department of Rensselaer Polytechnic Institute carried out a study to determine the effect of neutron irradiation on the noise and gain characteristics of GaAs MESFET microwave amplifiers. This report presents the results obtained during this research program.

The authors wish to acknowledge the help given by Messrs. M. L. Deane and L. F. Lowe during the irradiations at Hanscom AFB. The effort and time spent by Dr. P. J. Drevinsky while carrying out the neutron dosimetry is gratefully acknowledged. Special thanks are given to our contract monitor, Mr. H. M. DeAngelis, for the many technical discussions, suggestions and continued interest throughout the program. The diligence of Ms. Marita A. Jados while typing the reports and communications during the program are gratefully acknowledged.

## E V A L U A T I O N

This report is the final report of this contract. It covers research on the effects of radiation on the microwave properties of commercially available low noise GaAs MESFET devices during the period of 1 April 1978 to 30 June 1979. The effects of fast neutron and gamma irradiation on the signal and noise properties of microwave amplifiers implemented from these devices have been evaluated. The increase in noise figure has been related to the neutron-induced degradation in transconductance and an increase in the source resistance of the devices. The work performed under this contract provides data which is needed in assessing the use of low noise MESFET amplifiers in radiation-hardened systems.

  
HENRY M. DEANGELIS  
Project Engineer

## 1. INTRODUCTION

### 1.1 Introduction

Among the several microwave FET devices, the GaAs Schottky gate FET or MESFET is considered to be the most successful device for low noise and power amplification above 4 GHz. The reasons for this are the high value of low field mobility of GaAs and that the two critical dimensions of the FET, gate length and channel thickness, can be accurately controlled on high quality GaAs epitaxial layers which can now be grown on semi-insulating GaAs. Above 4 GHz, GaAs MESFETs have better efficiency as power amplifiers and lower noise figures as low noise amplifiers than bipolar transistors. Furthermore, the FETs do not exhibit secondary breakdown, are self-ballasting and have inherently higher input impedance.

The GaAs MESFET is not only capable of low-noise amplification and high efficiency power amplification and generation, but can be used for high speed logic as well as other microwave functions such as oscillators and mixers. In fact, there is a trend toward monolithic integration for digital, analog and hybrid applications. The monolithic approach is attractive because GaAs MESFETs fabricated on the same active layer can be used as switches, logic gates with active loads, amplifiers, oscillators and mixers, and the devices can be supported, isolated and interconnected with low parasitic capacitances on the semi-insulating substrate. It can be stated that the GaAs MESFET will have a large impact in the design of the microwave communication systems and high speed logic circuit within the next five to ten years.

The GaAs MESFET is less susceptible to radiation than other semiconductor devices since it is a majority carrier device, unlike the bipolar

transistor, and without any functional insulating layers like in MOS devices. However, recent experimental results<sup>(1)</sup> indicate that MESFET parameters such as transconductance, source resistance and output resistance do change with irradiation. Since the values of these parameters determine the noise and gain of MESFET amplifiers at microwave frequencies, a detailed documentation of radiation effects on the noise and signal characteristics of MESFET amplifiers is clearly needed before it can be used as a low noise amplifier in radiation hardened systems. In this report, we document the results of a research program carried out to investigate the effect of radiation on the signal and noise characteristics of low noise microwave GaAs MESFET amplifiers.

## 1.2 Program Outline

The program focused not only in the evaluation of the change on the microwave noise and signal characteristics of S- and X-band MESFET amplifiers but also on the change in the important MESFET parameters with radiation. Device parameters measured were microwave scattering parameters at S- and X-band, static I-V characteristics, 1 MHz small signal equivalent circuit parameters and low frequency noise between 1 KHz to 1.5 MHz. The evaluation of those parameters or characteristics was considered to be desirable in order to determine the causes of any change in the noise characteristics of the amplifiers tested. In Chapter 2 we describe the devices tested, the way in which the amplifiers were realized using commercial MESFET chips, the details of the microwave and low frequency measurement set ups and the radiation facilities and procedures used. Chapter 3 contains the radiation results and documents the changes in the microwave noise and signal characteristics of the

MESFET amplifiers tested as well as our interpretation of the causes of radiation induced changes observed. The last chapter summarizes the results of the program.

## 2. AMPLIFIERS TESTED AND MEASUREMENT PROCEDURES

### 2.1 Device Tested

Commercially available devices from three manufacturers, Hewlett Packard, Plessey and Nippon Electric were used for implementing the microwave amplifiers. The devices used were the HFET-1000 from Hewlett-Packard, the GAT-5 from Plessey and the NEC-244 from Nippon Electric. All of the above are low noise devices with one micron gate length, (except the GAT-5 which has a  $0.8\text{ }\mu\text{m}$  gate length) useful for small signal amplification up to X-band frequencies.

Using the above devices, microwave amplifiers were realized on alumina microstrip with the devices mounted in a common source configuration. The devices were obtained in chip form and mounted on a disc which was epoxyed to the microstrip. This "chip on a disc" mounting technique reduces the parasitic lead inductance between source bonding pad and microstrip ground which can deteriorate amplifier performance.<sup>2</sup> Figures 2.1 and 2.2 are schematics of the disc and of the microstrip line on which the disc is mounted. The disc on which the GaAs FET chip is bonded consists of a bottom disc 0.180" in diameter which has a post 0.050" in diameter and 0.017" high. The chip is mounted on the post using either insulating or silver conducting epoxy. The disc is bonded to the microstrip using conducting epoxy so that it makes contact to the ground plane. Connection between the device bonding pads and the microstrip were made by thermo-compression bonding 1 mil gold wire. Figure 2.3 is a photograph of a "chip-on-the-disc" with the device connected on the common source configuration. In order to protect the chip and its bonding wires during the testing and irradiations a plastic cap, cemented to the alumina substrate,



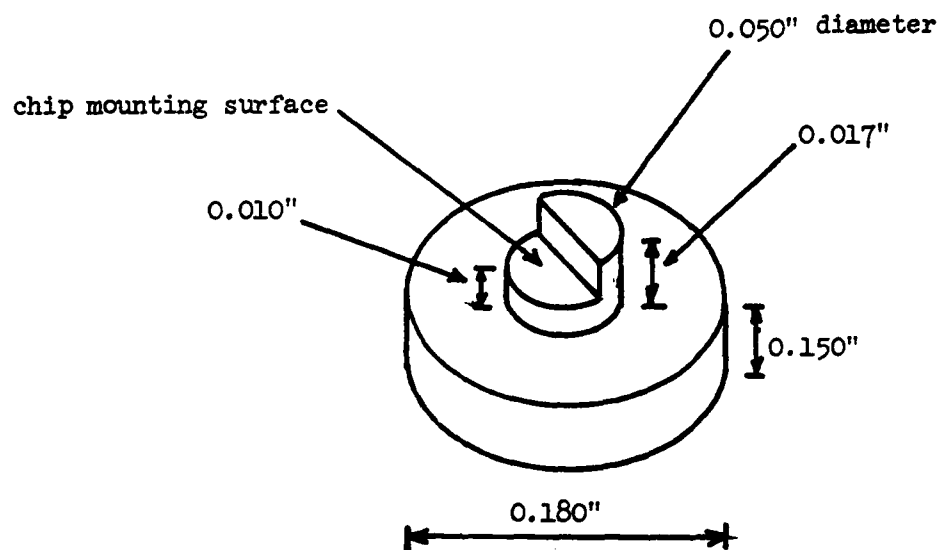


Fig. 2.1 Chip Mounting Disc

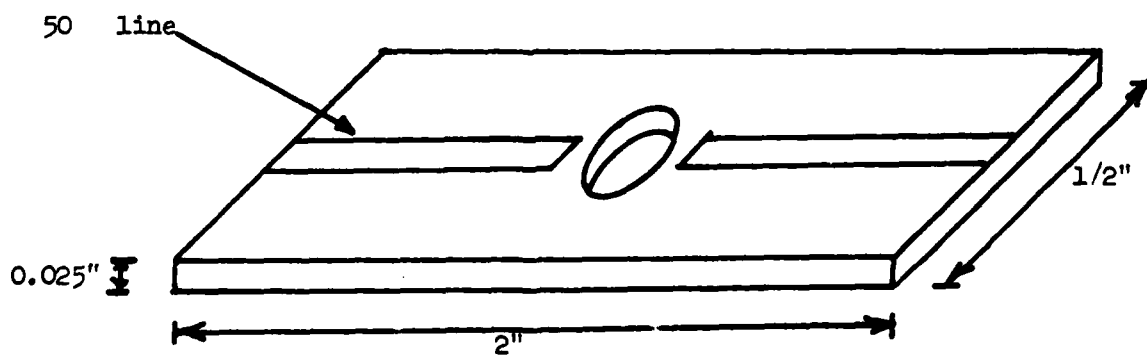


Fig. 2.2 Microstrip Device-Testing Structure

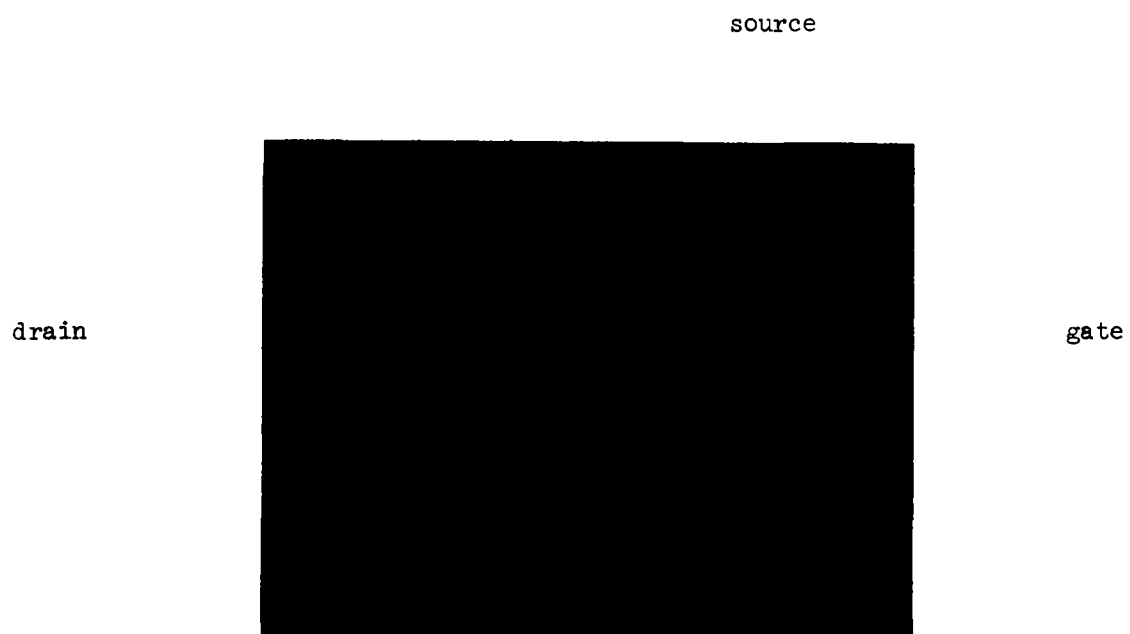


Fig. 2.3 GaAs FET Chip on Disc Showing Bonding Wires (chip dimensions  
0.025" x 0.011" x 0.005")

was placed on top of the device without affecting its electrical performance.

Using the above mounting technique S- and X-band amplifiers were implemented. Tuning of the input (gate) and output (drain) for minimum noise figure was accomplished by positioning discs along the  $50\ \Omega$  input and output microstrip lines.<sup>3</sup> The tuning discs behave, in the first approximation, as lumped capacitors which placed at the proper distance from the device ports allowed tuning for minimum noise figure. The length of the alumina substrate was chosen to be 2" so that at least half of a wavelength is available at both the input and output ports for placing the matching discs at S-band. The tuning discs were either epoxied to the microstrip making a semipermanent assembly or they could be positioned on the microstrip by means of a precision jig during microwave testing. The advantage of using the above mounting configuration is that it allows measurement of the scattering parameters of the device with the tuning discs removed. Once those measurements have been carried out, the tuning discs are properly placed over the microstrip and an amplifier is obtained (the discs can be cemented to the alumina to have a semipermanent assembly). The gain and noise characteristics of the amplifier can then be measured. If necessary, the discs can be removed to measure changes in the scattering parameters of the device after any of the irradiations. Figures 2.4 and 2.5 are photographs of an S- and X-band amplifiers respectively. The pictures show that the discs used for tuning at X-band are smaller than the ones used at S-band. Using commercial devices such as HFET-1000 from Hewlett-Packard GAT-5 from Plessey and NEC-244 from Nippon Electric, amplifiers with 14 dB gain and noise figure (NF) of 2.1 dB at

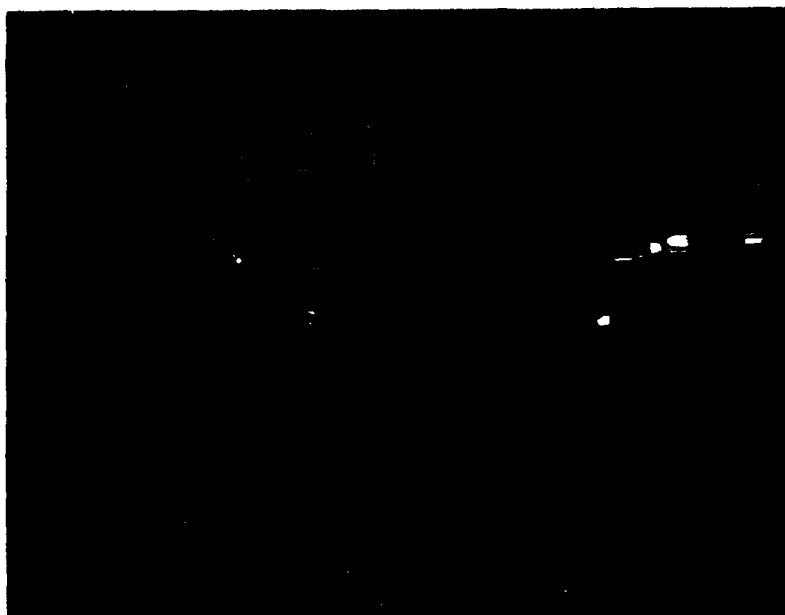


Fig. 2.4 S-Band Amplifier with Tuning Discs

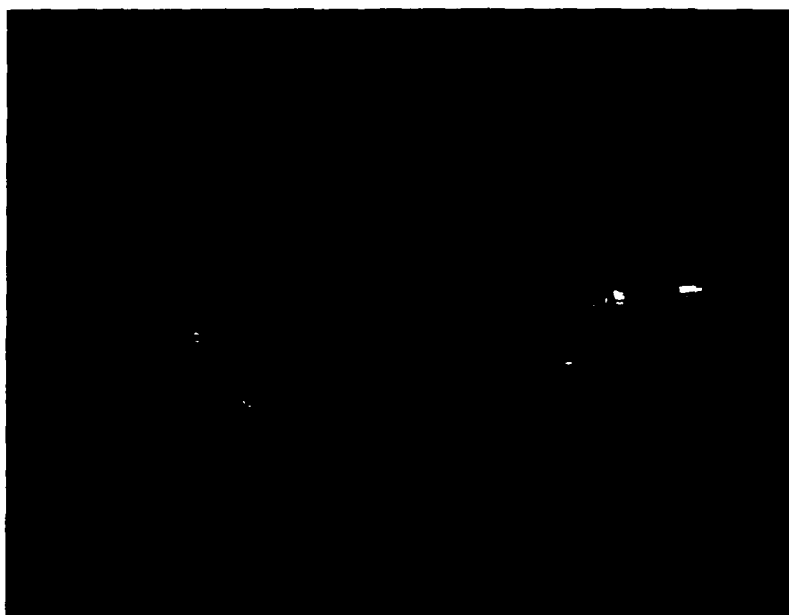


Fig. 2.5 X-Band Amplifier with Tuning Discs and Protective Cap over Chip

3 GHz and 8 dB gain and 2.9 NF at 9 GHz were realized. Typical bandwidths were 200 MHz for a change of 0.3 dB in NF with a corresponding change of  $\pm 2$  dB in the amplifier gain.

## 2.2 Low Frequency Measurements

Low frequency testing consisted of the measurement of the DC characteristics drain current  $I_D$  vs. drain voltage  $V_D$  as a function of gate voltage  $V_G$ , of the 1 MHz voltage gain and of the low frequency noise between 1 KHz and 1.5 MHz. Figure 2.6 shows a schematic diagram used for the DC and 1 MHz characterization of the GaAs MESFET. The set-up consisted of a Princeton Applied Research Model 410 C-V plotter, a special purpose ramp generator for sweeping the drain voltage, an RF voltmeter with DC analog output and the MESFET mounted in the same jig used in the microwave measurements described previously. By operating the above set-up in conjunction with an X-Y recorder, real time plots of drain current vs. drain voltage, 1 MHz voltage gain vs. drain voltage could be produced for several values of gate to source voltages. The data was recorded on 11" x 15" graph sheets which allowed for good resolution in reducing the data.

The drive terminal of the PAR-410 C-V plotter supplied the gate-to-source DC bias voltage as well as the 1 MHz small signal voltage (15 mV rms) for the voltage gain measurements. The measurement circuit was designed to prevent any instabilities with output loads  $R_L$  ranging from 10 ohms to open circuited conditions. This was achieved by mounting the several components (low inductance resistors and capacitors) in 50 ohm coaxial connectors and placing a 300 pF capacitor between drain and source. The output of the ramp generator had a filter which, in combination

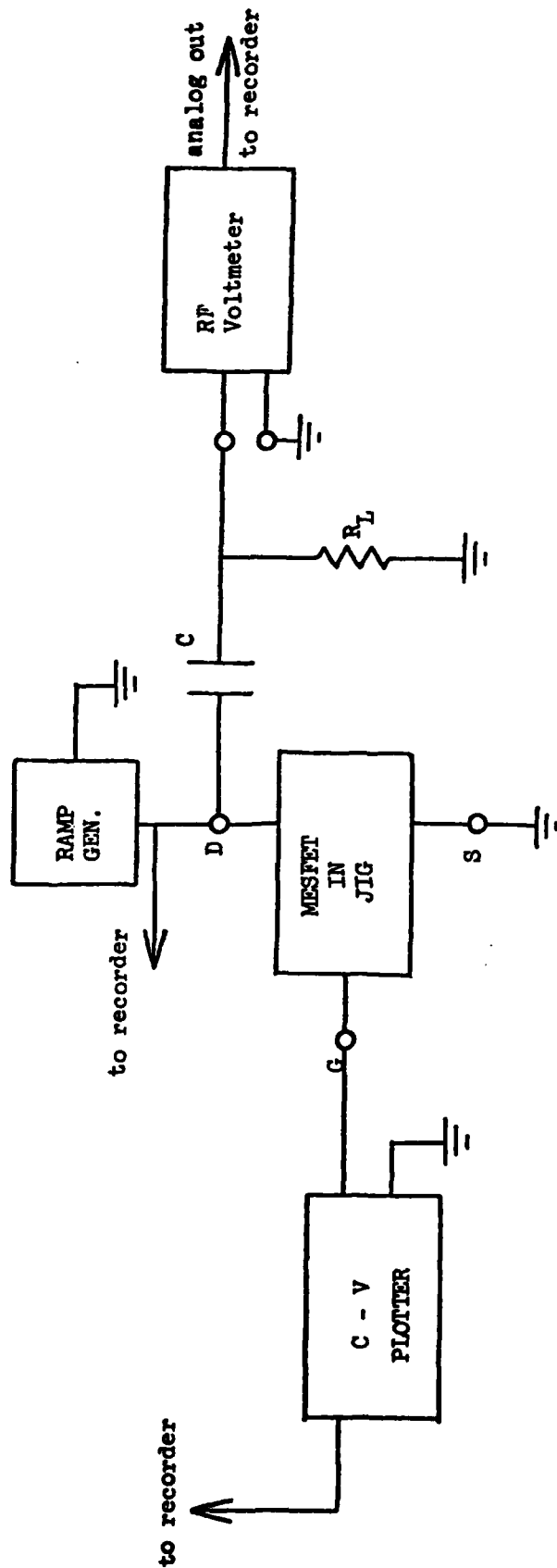


Fig. 2.6 Schematic of Low-frequency Test Set-up

with the 300 pF capacitor, prevented any loading of the drain terminals at 1 MHz.

Low frequency noise measurements were carried out in the same set up except that the C-V plotter was substituted by a filtered battery to provide gate bias and a low noise 50  $\Omega$  resistor, in series with a by pass capacitor, was used for terminating the gate to source terminals. The value of the load resistor  $R_L$  used was of the order of 500  $\Omega$  so that the low frequency voltage gain of the MESFET amplifier was of the order of 10 at zero gate bias. During the measurements the voltage of the ramp generator was kept constant at 3 volts so that the devices were in saturation. In the above set up the RF voltmeter served as a low noise wide band amplifier with a gain of 100. The voltmeter was followed by an HP-310A wave analyzer which measured the noise voltage. The above set up was also automated and if operated in conjunction with an X-Y recorder real time plots of noise voltage vs. frequency could be recorded for several values of gate voltage.

### 2.3 Microwave Measurements

Microwave measurements emphasized amplifier noise and gain measurements at both S- and X-bands. In a few cases the microwave scattering parameters of the devices were measured by removing the tuning discs of the amplifier, which had been epoxied to the microstrip. In those cases any additional amplifier measurements were carried out by positioning the tuning discs, on the input and output lines, with a special microstrip jig.

Figure 2.7 is a schematic diagram of the S-band amplifier noise and gain measurement set up. The set up has the capability of amplifier noise

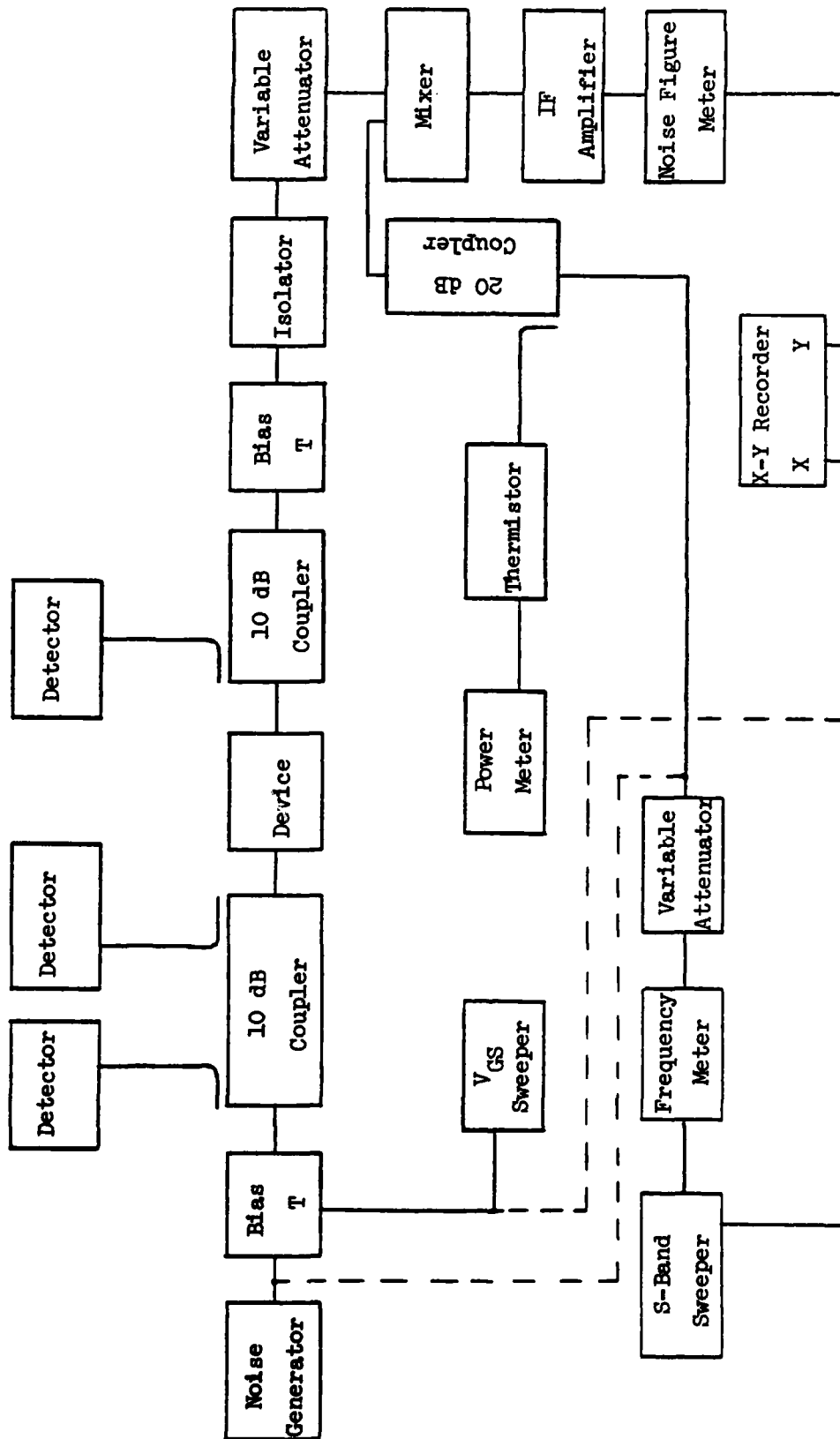


Fig. 2.7 Schematic Diagram of S-band Amplifier Noise and Gain Measurement Set up



and gain measurement as a function of frequency and as a function of gate bias. The key components of the set up are: a broad (1-12.4 GHz) solid state noise source (Ailtech Mod. 7616), an S-band mixer (Ailtech Model 13505), a 30 MHz IF amplifier with a 3 MHz noise bandwidth (Ailtech Model 13639) and a Precision Noise Figure Indicator (Ailtech Model 7512C). The above set up measures the noise figure by the Y-factor method with an accuracy and reproducibility better than 0.1 dB. The minimum noise figure that can be measured is determined by the noise of the mixer - IF amplifier combination (second stage contribution) and the gain of the amplifier being evaluated. The noise figure of the second stage (mixer plus IF amplifier) is 6.8, 6.6 and 11.6 dB at 2, 3 and 3.8 GHz. For amplifiers with a 15 dB of gain, the noise contributed by the second stage is 0.5, 0.46 and 1.5 dB at the above specified frequencies. This indicates that noise figures as low as 0.1 to 0.5 dB can be measured in amplifiers with a gain of 15 dB in the S-band frequency range.

The same noise measurement components, except for an X-band mixer, Ailtech Model 13546, instead of an X-band mixer were used for measuring noise at X-band. Figure 2.8 is a schematic diagram of the X-band amplifier noise and gain measurement setup, which was also used for device scattering parameter evaluation. Three 4-port transfer switches were used so that these measurements could be performed with no critical connections having to be changed. As shown the setup is used for noise figure measurements. With both  $S_1$  and  $S_2$  switched, a gain measurement is possible, the gain reference being taken by switching  $S_3$ . The second stage noise figure (from 10 dB coupler at device under test output "back") is 8 to 10 dB from

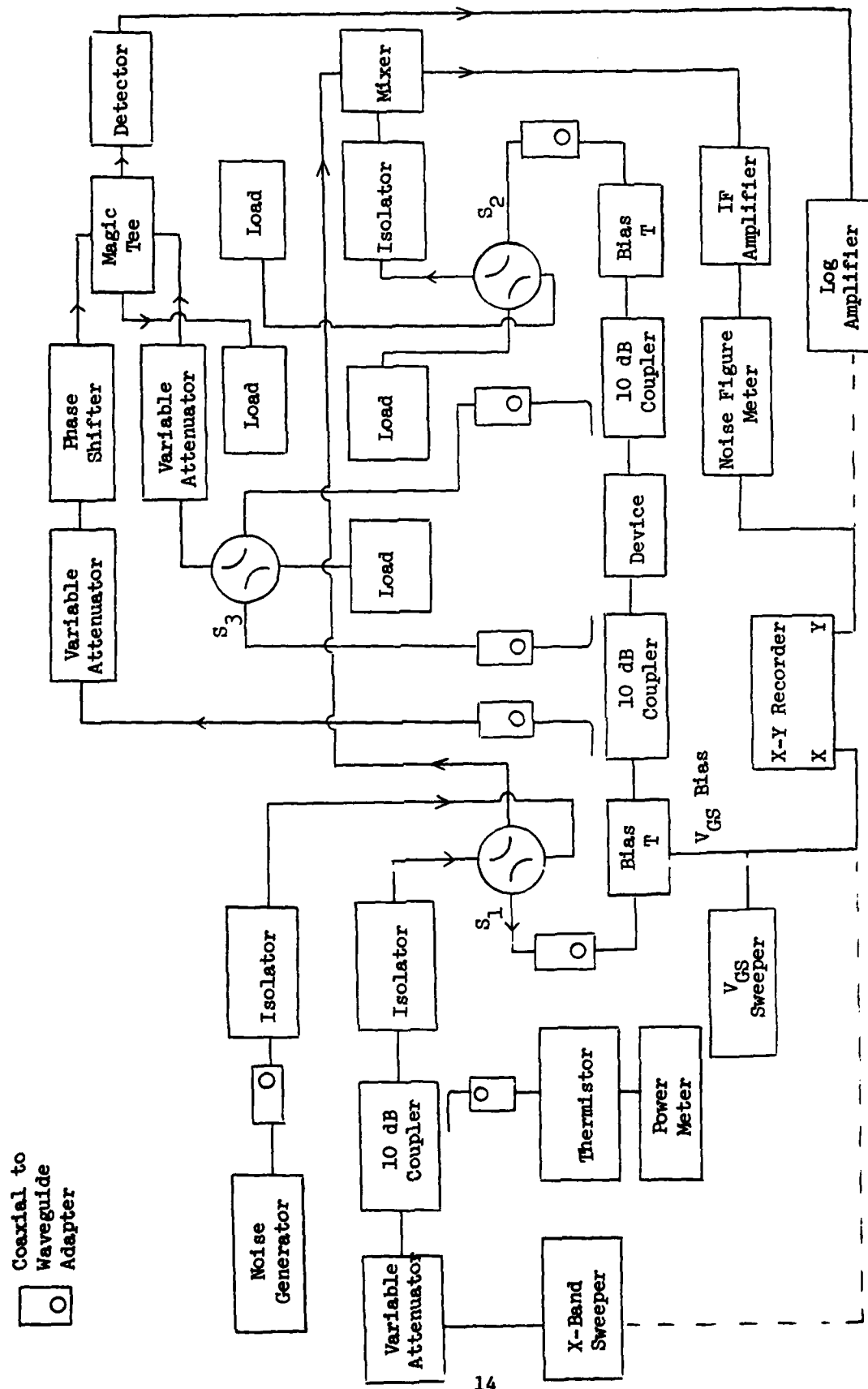


Fig. 2.8 X-Band Amplifier (Gain and Noise Figure) and Device (Scattering Parameter) Measurement Setup

9 to 11 GHz, which results in a significant noise contribution with the lower gain X-band amplifiers. However the measurement reproducibility, a key factor in the program, was not adversely affected.

Figure 2.9 shows the microwave bridge used for scattering parameter measurements at S-band. The bridge is used in a conventional manner to obtain the 4 scattering parameters. Precision 7 mm connectors were used in the critical test components and the 7 mm to microstrip launchers were the only adapters used in the circuitry which could affect measurement precision. The phase shifter utilized was a Narda Model 3752 and the attenuators were a Weinnchel Model 953 and an Alfred Model E103. With this test set up a gain and phase accuracy of  $\pm 0.3$  dB and  $\pm 2.0^\circ$  was achieved.

#### 2.4 Radiation Testing

The amplifiers were exposed to neutron and  $\gamma$ -radiation. Two different neutron sources were used. One of them was the Van de Graaff accelerator of the Solid State Sciences Division RADC/ES at Hanscom Air Force Base, MA which produced a 5.5 MeV monoenergetic neutron beam. With this neutron source the devices were exposed to total fluences in the range of  $3 \times 10^{12}$ ,  $8 \times 10^{12}$  and  $2 \times 10^{13}$  n/cm<sup>2</sup> as determined by sulfur pellet dosimetry. The second neutron source used was the water moderated Biomedical Research Reactor at Brookhaven National Laboratory which has a fission type spectrum. The neutron fluences with this source were  $1 \times 10^{14}$ ,  $4 \times 10^{14}$  and  $1 \times 10^{15}$  n/cm<sup>2</sup>.

The  $\gamma$ -irradiations were carried out at the Co<sup>60</sup> source facility at Hanscom AFB. In this case the devices were exposed to a total dose of  $2 \times 10^7$  rads (Si). No other doses were used since from the previous program<sup>1</sup> we had determined that all the device signal characteristics

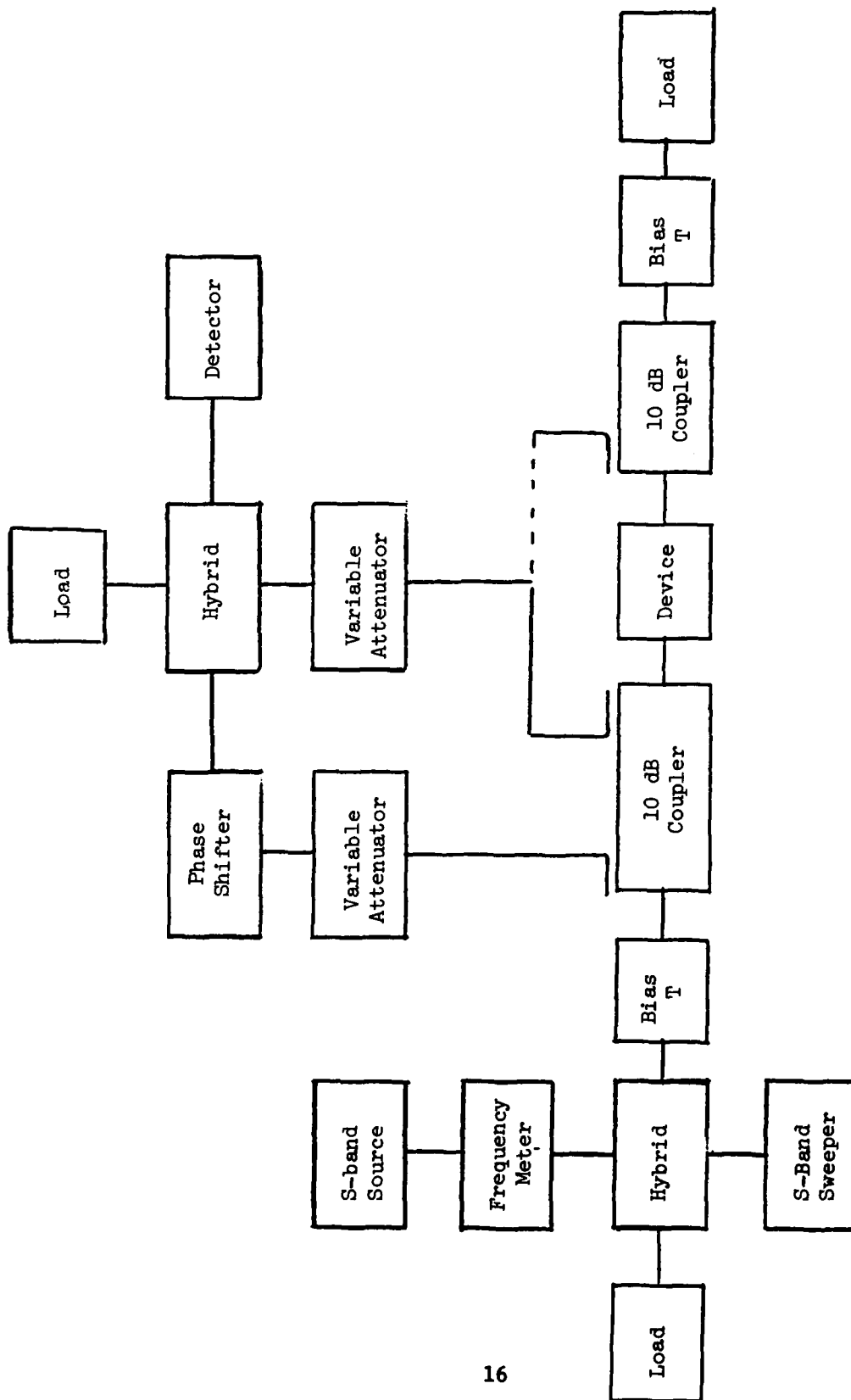


Fig. 2.9 Schematic Diagram of S-band Scattering Parameter Measurement Set-up

were very insensitive to  $\gamma$ -radiation up to  $8 \times 10^7$  rads (Si). During all the irradiations, both neutron and gamma, the devices were unbiased and their temperature was below  $30^\circ\text{C}$ . Amplifier characterization was carried out before and after each irradiation. Usually the measurements were carried out one or two days after the amplifier had been irradiated, except during the first two irradiations of the program. During those irradiation low frequency characterization and S-band noise measurements were done one or two hours after device irradiation. No X-band measurements were done in this case.

Table 2.1 is a summary of the six irradiations performed in the seven amplifiers tested during the program. The first irradiation was done mainly with the purpose of testing our instrumentation. The second irradiation was designed for determining changes in amplifier characteristics at low neutron fluences ( $10^{12}$  to  $10^{13}$  n/cm<sup>2</sup>) using the mono-energetic neutron beam of the Van de Graaff accelerator. Irradiations 3, 4 and 5 were done at the Brookhaven facility which provided a higher neutron fluence in a shorter time. The last irradiation, No. 6, was used to determine the effect of  $\gamma$ -dose in amplifier characteristics. It was done on amplifiers which had been irradiated at a low neutron fluence because their characteristics had not changed by any appreciable amount. The changes observed during the irradiations were so consistent that it was not necessary to test more than the seven amplifiers shown.

Table 2.1 - Radiation Summary \*

Device	Hanscom AFB (n/cm <sup>2</sup> )		Brookhaven (n/cm <sup>2</sup> )			Hanscom AFB	
	Irrad. 1	Irrad. 2	Irrad. 3	Irrad. 4	Irrad. 5	Irrad. 6	
NEC-244-31	3x10 <sup>12</sup>	8.3x10 <sup>12</sup> 1.9x10 <sup>13</sup>	-	4x10 <sup>14</sup>	1x10 <sup>15</sup>	-	
GAT-5-48	-	2.1x10 <sup>12</sup> 6.5x10 <sup>12</sup> 1x10 <sup>13</sup>	1x10 <sup>14</sup>	4x10 <sup>14</sup>	1x10 <sup>15</sup>	-	
HFET-1000-44	-	6.3x10 <sup>12</sup> 1.5x10 <sup>13</sup>	1x10 <sup>14</sup>	4x10 <sup>14</sup>	1x10 <sup>15</sup>	-	
GAT-5-43	-	2.1x10 <sup>12</sup> 6.5x10 <sup>12</sup> 1x10 <sup>13</sup>	-	-	-	2x10 <sup>7</sup> rads(Si)	
NEC-244-35	-	2.5x10 <sup>12</sup> 6.1x10 <sup>12</sup>	-	-	-	2x10 <sup>7</sup> rads(Si)	
NEC-244-32	-	2.5x10 <sup>12</sup> 6.1x10 <sup>12</sup>	-	-	-	4.5x10 <sup>13</sup> n/cm <sup>2</sup>	
NEC-244-49	-	-	-	-	6x10 <sup>14</sup>	-	

\* Neutron fluences are total at each facility.

### 3. RESULTS AND DISCUSSION

#### 3.1 Introduction:

In this chapter we summarize the radiation results and present our interpretation of the causes of the radiation induced changes in amplifier signal characteristics. The results are presented in the same order as the one in which they were obtained during the program; first the low neutron fluence irradiation results, then the results obtained with the high neutron fluence irradiation and last the  $\gamma$ -dose irradiation results.

#### 3.2 Low Neutron Fluence Results:

As shown in the Radiation Summary given in Table 2.1 page 18, irradiation #2 was carried out for determining the effect of low neutron fluence on amplifier signal characteristics and it was done using the 5.5 MeV neutron source at Hanscom AFB. For fluences below  $1 \times 10^{13}$  n/cm<sup>2</sup>, the change in any of the low frequency characteristics was less than 2% or 3% and no change was observed on the microwave amplifier noise or gain. This was consistently observed in all the 6 amplifiers tested. Measurable changes in some of the low frequency characteristics were observed in device NEC-244-32 which was irradiated to a fluence of  $4.5 \times 10^{13}$  n/cm<sup>2</sup> at the end of the program (Irradiation #6). Fig. 3.1 shows the DC  $I_D$  vs.  $V_D$  characteristics before and after irradiation. The saturated drain current decreased approximately 5mA for gate biases close to zero. No change was observed in the transconductance  $g_m$  nor in the microwave noise figure although a change was observed in the low frequency noise. Fig. 3.2 shows the low frequency equivalent input noise voltage in the frequency range 1 kHz - 1.5 MHz at zero gate bias before and after irradiation. The decrease in the saturated drain current and the increase in the low frequency noise indicate that some

NEC-244-32

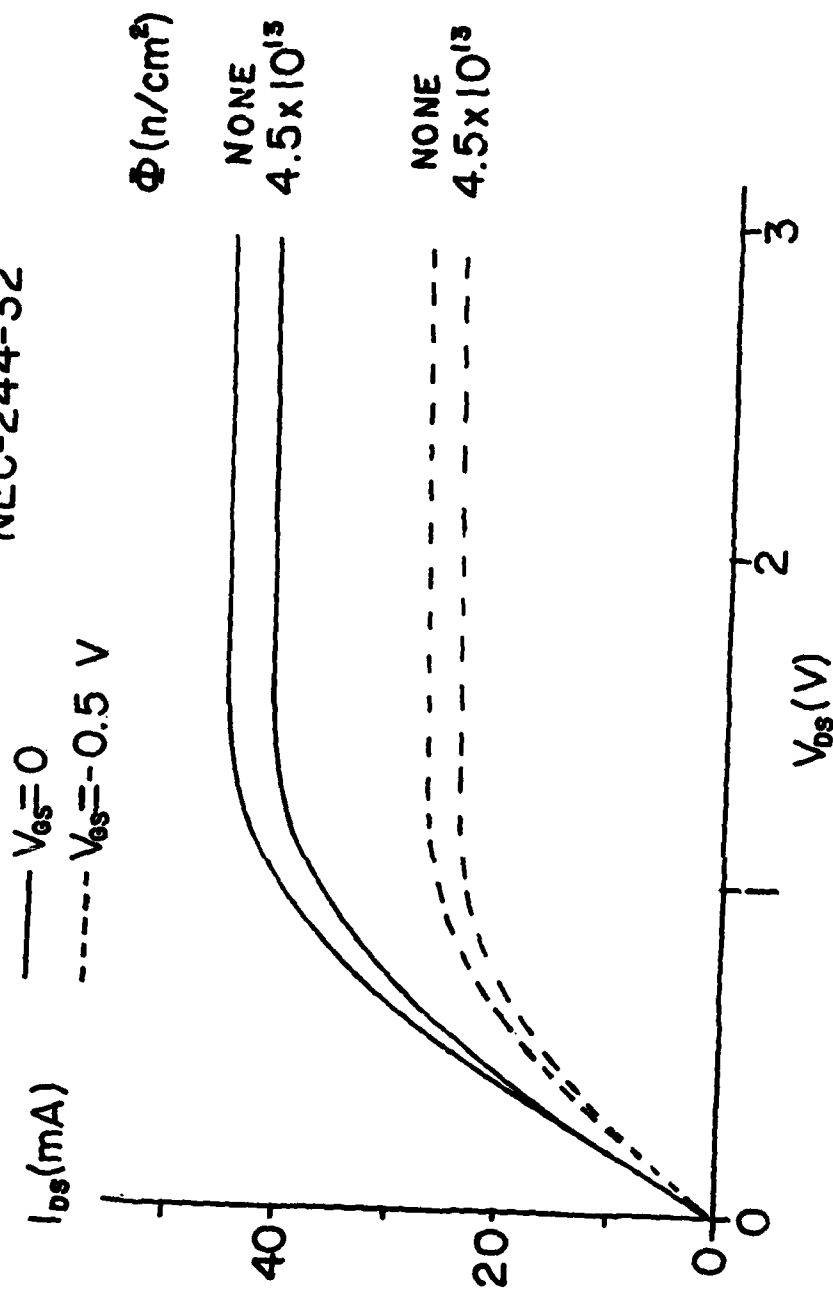


FIG. 3.1 - CHANGE IN THE DRAIN CURRENT VS. DRAIN VOLTAGE DC CHARACTERISTICS AT LOW NEUTRON FLUENCES.



NEC-244-32

$V_{DS} = 3V$ ,  $V_{GS} = 0V$



FIG. 3.2 - CHANGE IN THE LOW FREQUENCY EQUIVALENT NOISE INPUT VOLTAGE.

trap levels have been introduced which produce some compensation in the channel and which increase the low frequency noise. These traps apparently do not respond at microwave frequencies since the microwave noise figure was not increased.

### 3.3 Changes in Low Frequency Characteristics at High Neutron Fluences:

Figs. 3.3, 3.4 and 3.5 show the DC  $I_D$  vs.  $V_D$  characteristics of the three devices NEC-244-31, GAT-5-48 and HFET-1000-44 which were irradiated at the Brookhaven facility to total neutron fluences of  $1 \times 10^{14}$ ,  $4 \times 10^{14}$  and  $1 \times 10^{15}$  n/cm<sup>2</sup>. The characteristics for the first dose are not given because the change in the saturated drain current at zero bias was of the order of 1 to 2 mA for the three devices. Notice that the changes in saturated drain current are very similar in all the devices being highest for the GAT-5-48 which had the highest pre-irradiation drain current. For fluence above  $10^{14}$  n/cm<sup>2</sup> there is appreciable degradation in the saturated drain current and a decrease in the magnitude of the gate pinch-off voltage as determined by plotting  $\sqrt{I_D}$  versus gate voltage and extrapolating to zero current. For example for NEC-244-31 the pinch-off voltage decreased to 1.2 volts after  $1 \times 10^{15}$  n/cm<sup>2</sup> from an initial value of 1.5 volts before irradiation.

It is interesting to compare the change in saturated drain current shown in Fig. 3.1 for the NEC-244-32 with the one shown in Fig. 3.3 for the NEC-244-31 since each was irradiated with different neutron spectrum. Assuming that percent changes in the saturated drain current at zero bias are proportional to the damage introduced, it is found that 5.5 MeV neutrons at the Hanscom facility are 5 to 8 times more effective in producing damage than the neutrons at Brookhaven. This number is reasonable since the radiation damage equivalent of 5.5 Me V in silicon is around 2.

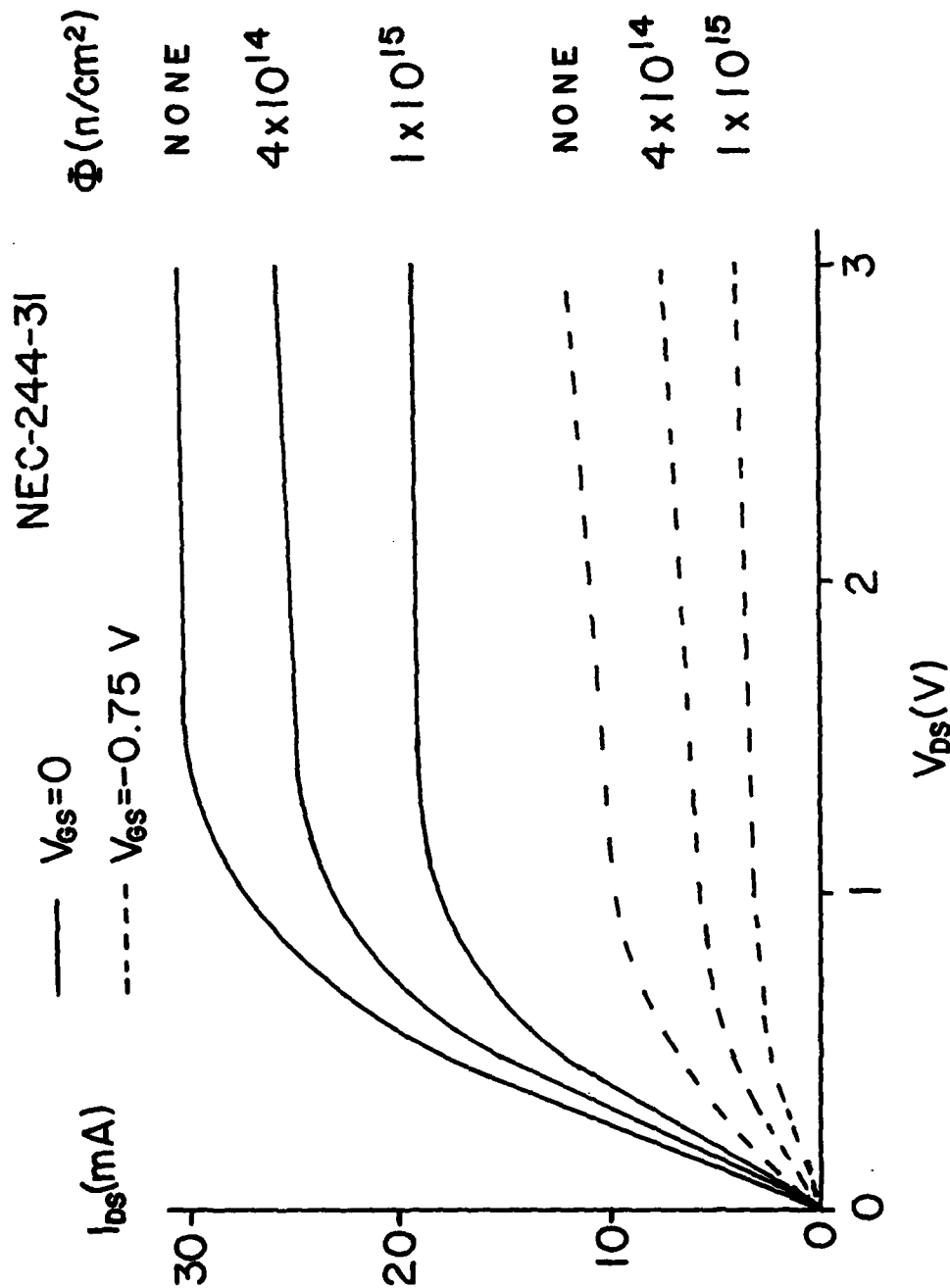


FIG. 3.3 - DRAIN CURRENT VS. DRAIN VOLTAGE DC CHARACTERISTICS AFTER HIGH NEUTRON FLUENCES.

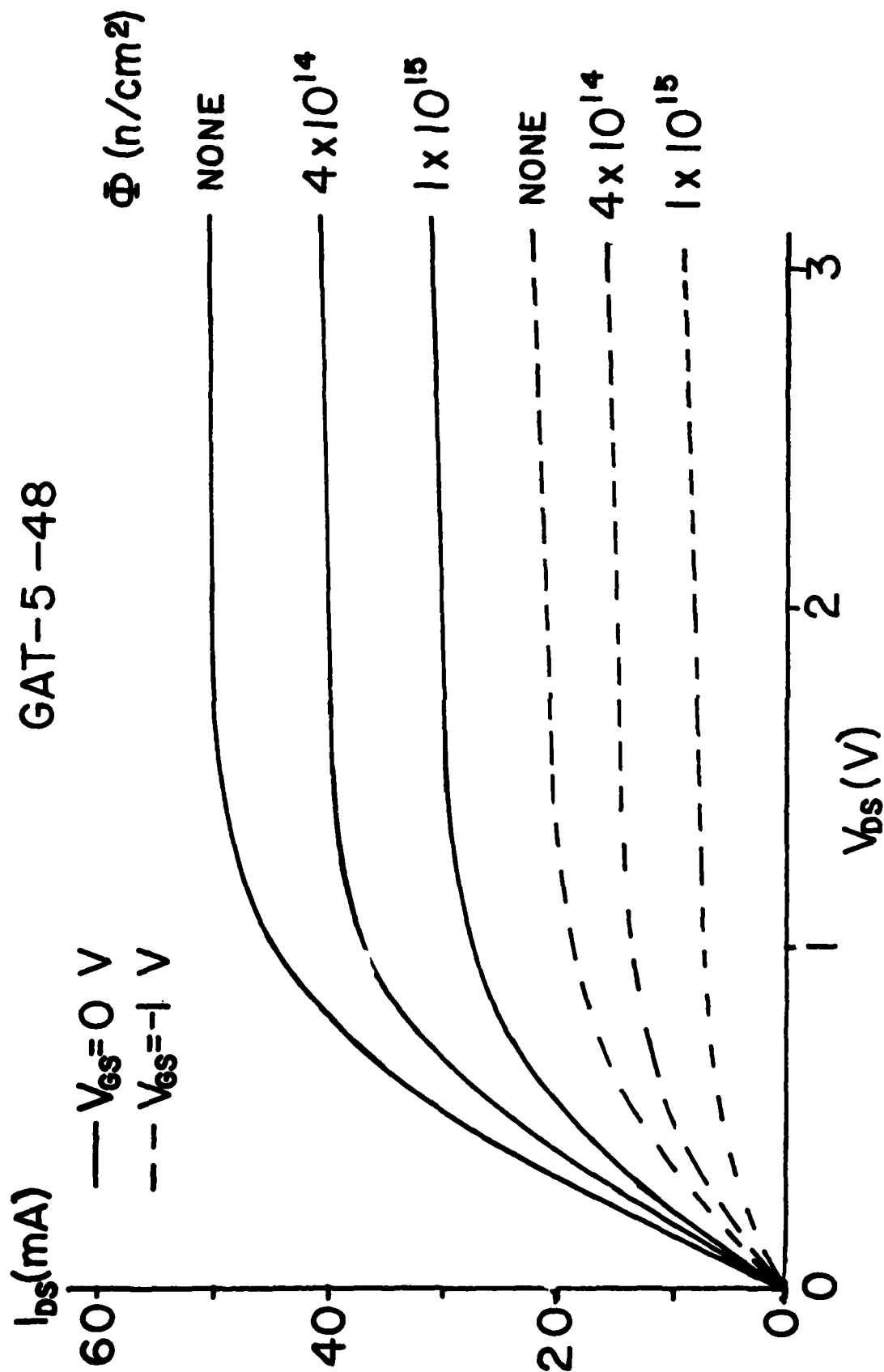


FIG. 3.4 - DRAIN CURRENT VS. DRAIN VOLTAGE DC CHARACTERISTICS AFTER HIGH NEUTRON FLUENCES.

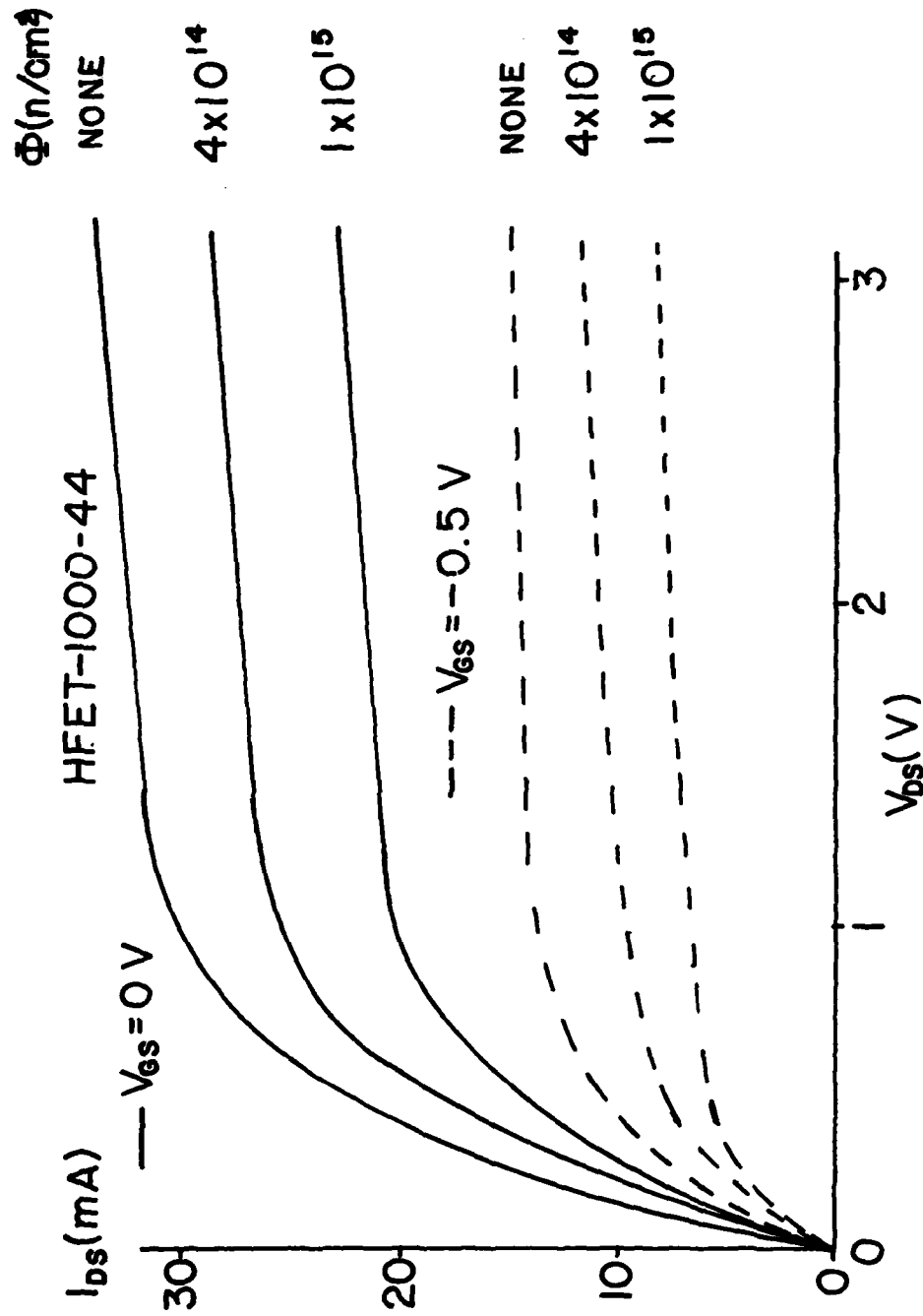


FIG. 3.5 - DRAIN CURRENT VS. DRAIN VOLTAGE DC CHARACTERISTICS AFTER HIGH NEUTRON FLUENCES.

Figures 3.6, 3.7 and 3.8 show the low frequency (1 MHz) transconductance  $g_m$  before and after irradiation to  $1 \times 10^{15}$  n/cm<sup>2</sup> for the three devices. Notice that at zero gate bias the change in this parameter is not as large as the one observed in the drain current. The change in the transconductance occurs at reverse bias which is consistent with the fact that the pinch-off voltage has decreased. The large change observed in the saturated drain current and the smaller change observed in the zero gate bias transconductance are due to the non-uniform doping of the active channel as explained previously.<sup>1</sup>

Figs. 3.9, 3.10 and 3.11 show the change in low frequency equivalent input noise voltages between 1 KHz - 1.5 MHz at reverse gate bias. The data is presented for a single neutron fluence. Similar results were obtained at other neutron fluences.<sup>4</sup> The noise power spectrum has approximately 1/f frequency dependence and the noise voltage increases by a factor of 2 to 3. This increase in noise voltage is appreciable and indicates that the deep levels introduced produce noise above the noise due to the deep levels present before irradiation. The increase in noise voltage at zero gate bias was less than at reverse bias indicating that the noise increases with the size of the depletion layer in the active layer of the device.

#### 3.4 Changes in Microwave Noise and Gain at High Neutron Fluences:

Figs. 3.12 to 3.17 show the noise figure and transducer power gain as a function of reverse gate bias at a frequency of 3 GHz (to insure reproducibility in the data, the tuning discs of these three S-band amplifiers were epoxied to the microstrip after positioning for minimum noise figure at 3 GHz before irradiation). Notice that there is a monotonic increase in the minimum noise figure with neutron fluence and that this minimum shifts to a lower value of gate bias. This shift is caused by the decrease in pinch-off voltage as

NEC-244-31

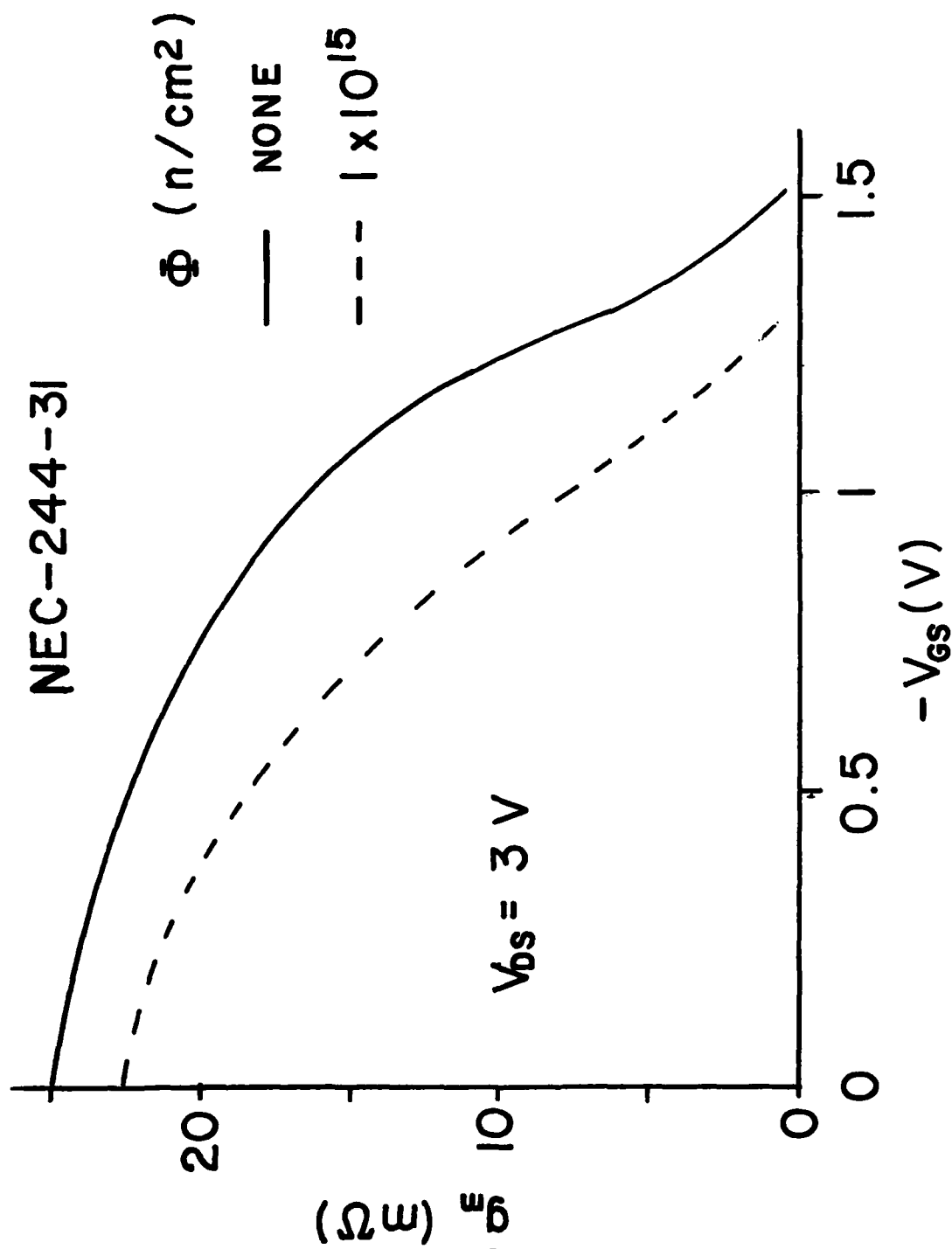


FIG. 3.6 - 1 MHz TRANSCONDUCTANCE VS. GATE VOLTAGE CHARACTERISTICS AFTER HIGH NEUTRON FLUENCE.

GAT-5-48

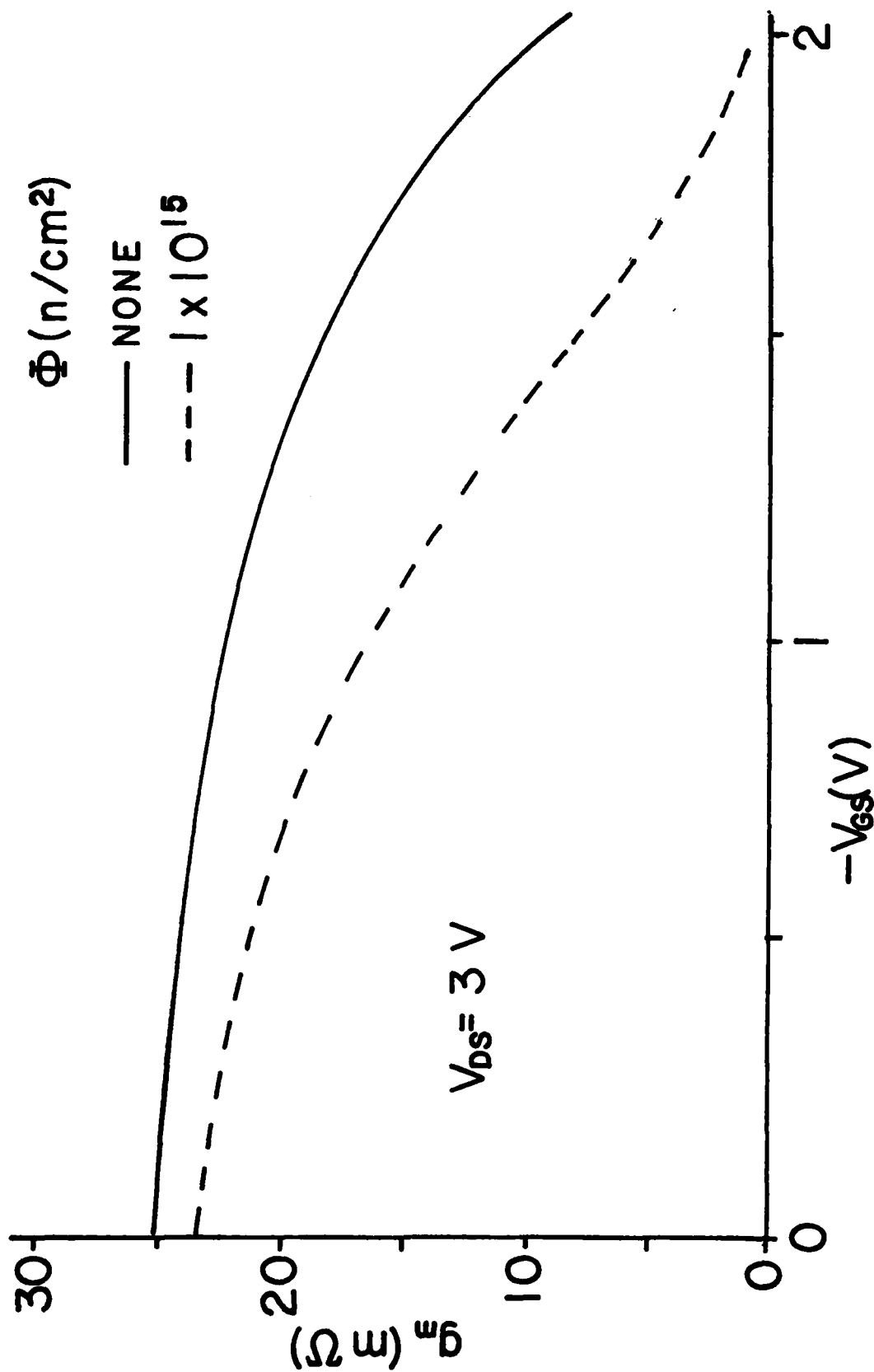


Fig. 3.7 - 1 MHz Transconductance vs. Gate Voltage Characteristics after High Neutron Fluence.



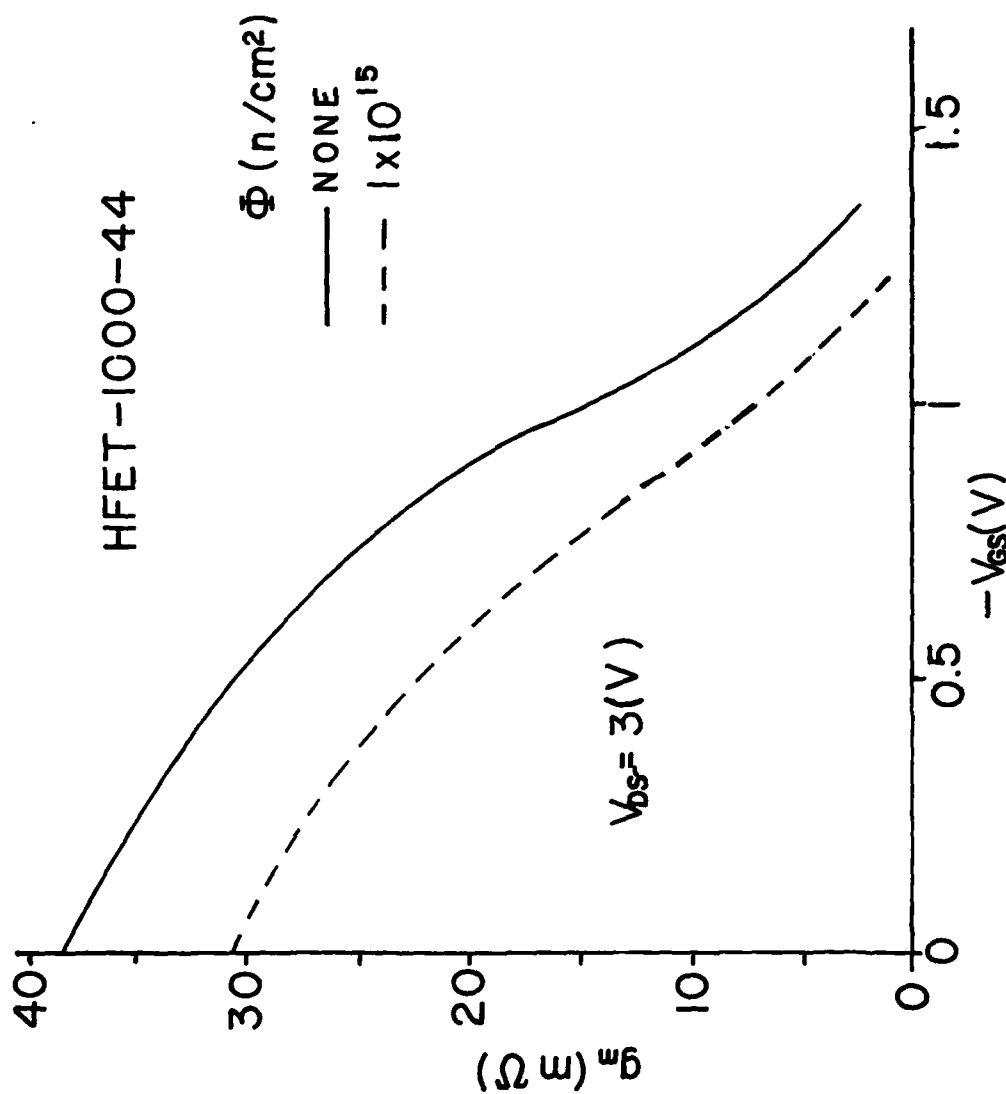


Fig. 3.8 - 1 MHz Transconductance vs. Gate Voltage Characteristics  
After High Neutron Fluence.

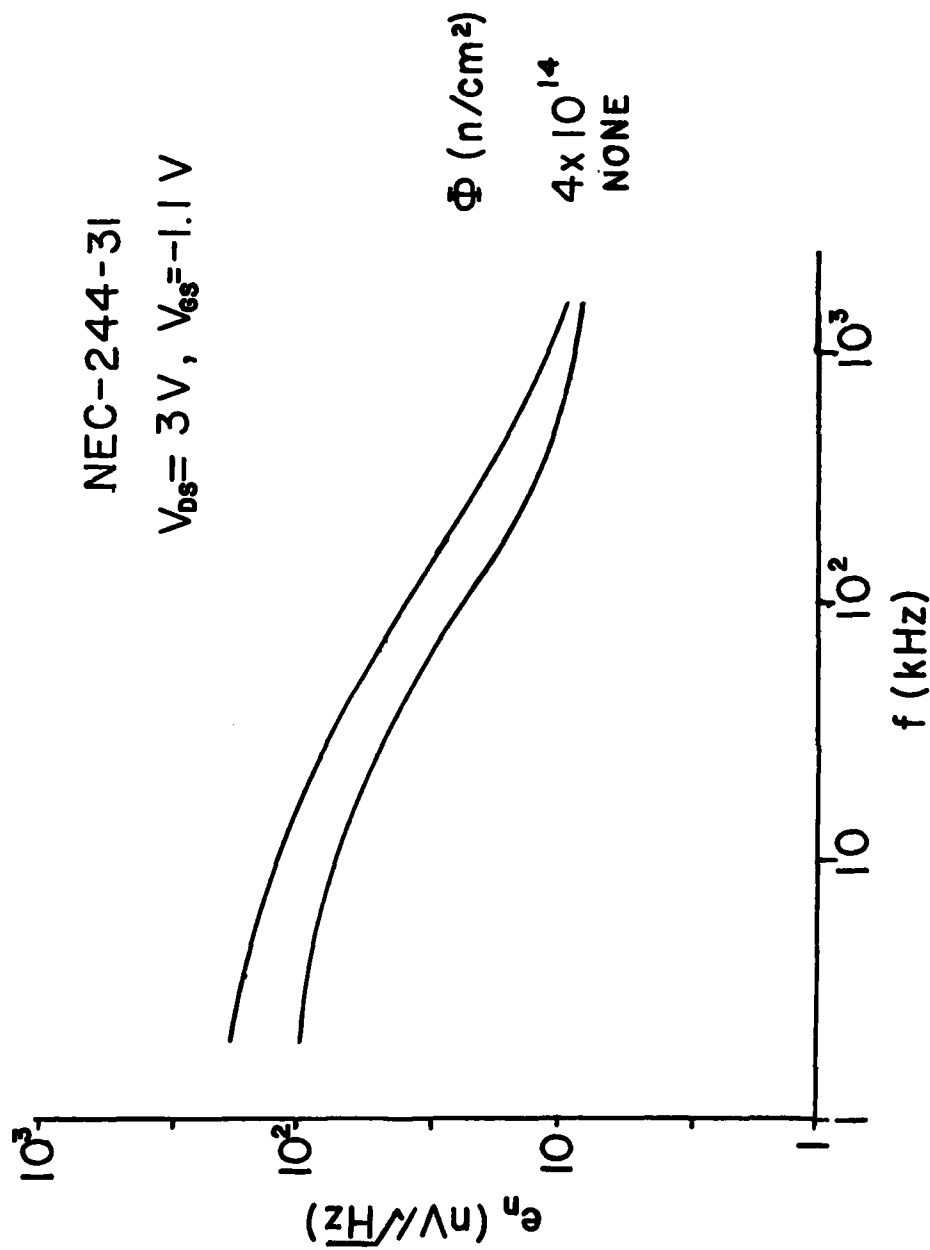


FIG. 3.9 - Low Frequency Equivalent Noise Input Voltage as a Function of Frequency AFTER HIGH NEUTRON FLUENCE.

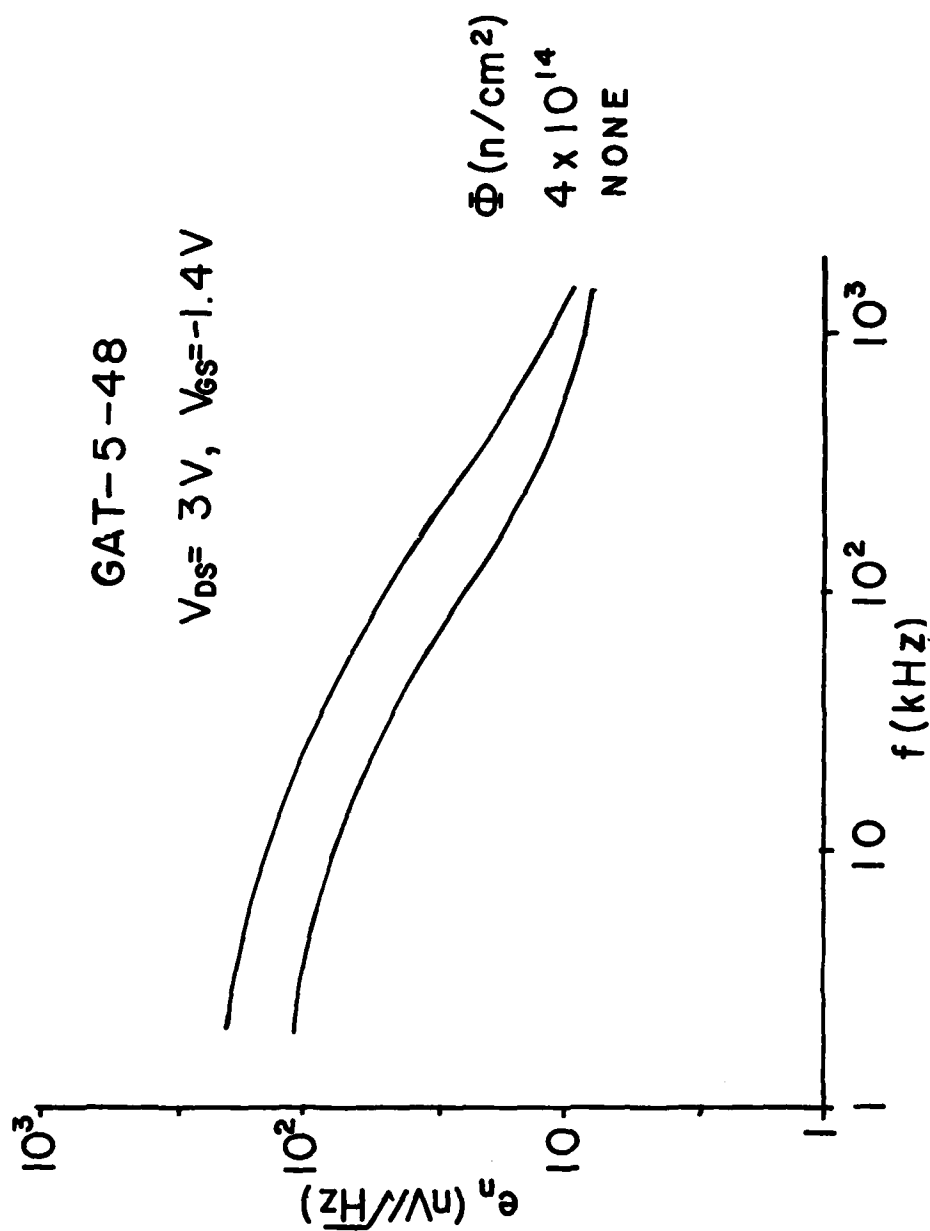


FIG. 3.10 - LOW FREQUENCY EQUIVALENT NOISE INPUT VOLTAGE AS A FUNCTION OF FREQUENCY AFTER HIGH NEUTRON FLUENCE.

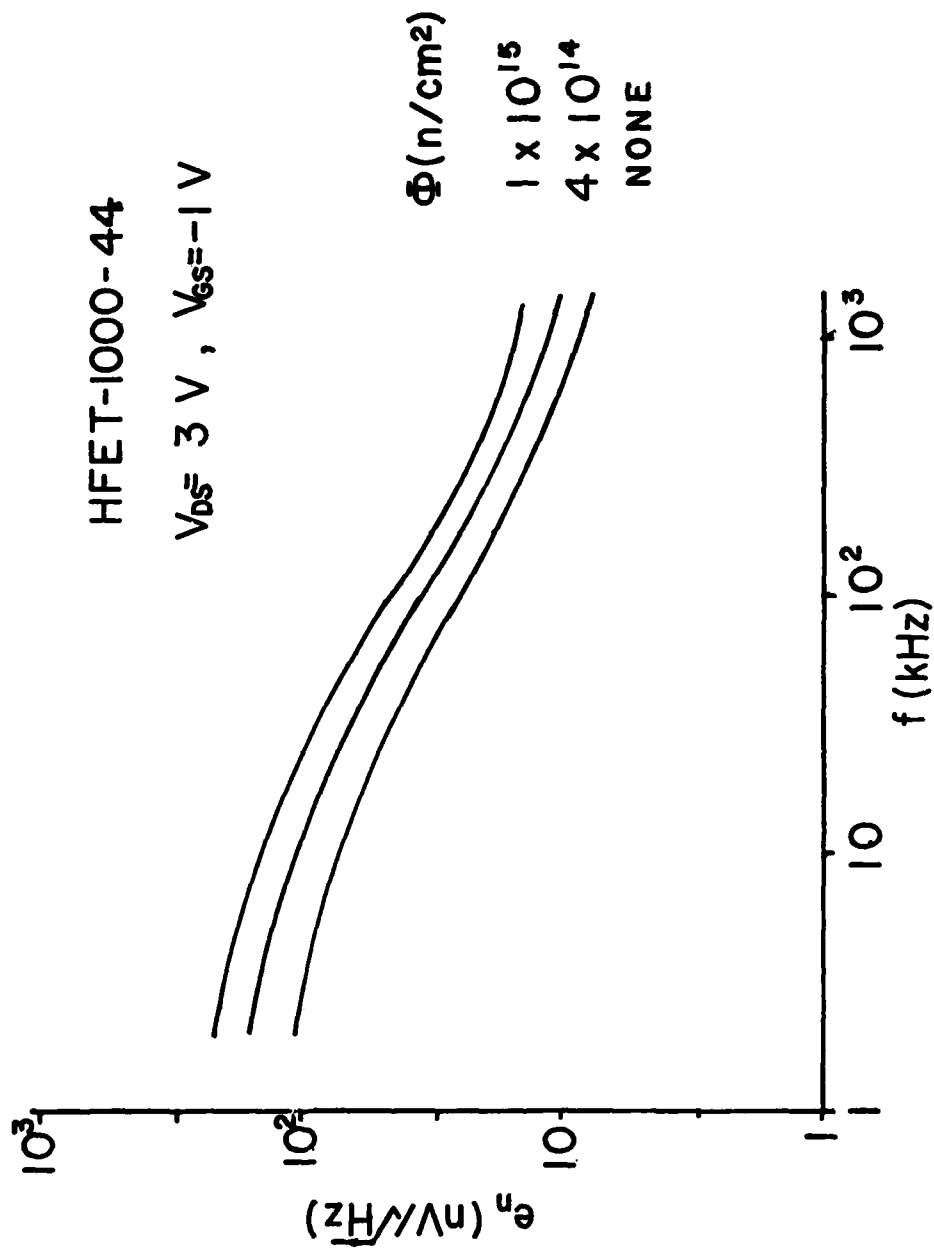


Fig. 3.11 - Low Frequency Equivalent Noise Input Voltage as a Function of Frequency after High Neutron Fluence.

NEC-244-3I

$f = 3 \text{ GHz}$   
 $V_{DS} = 3 \text{ V}$

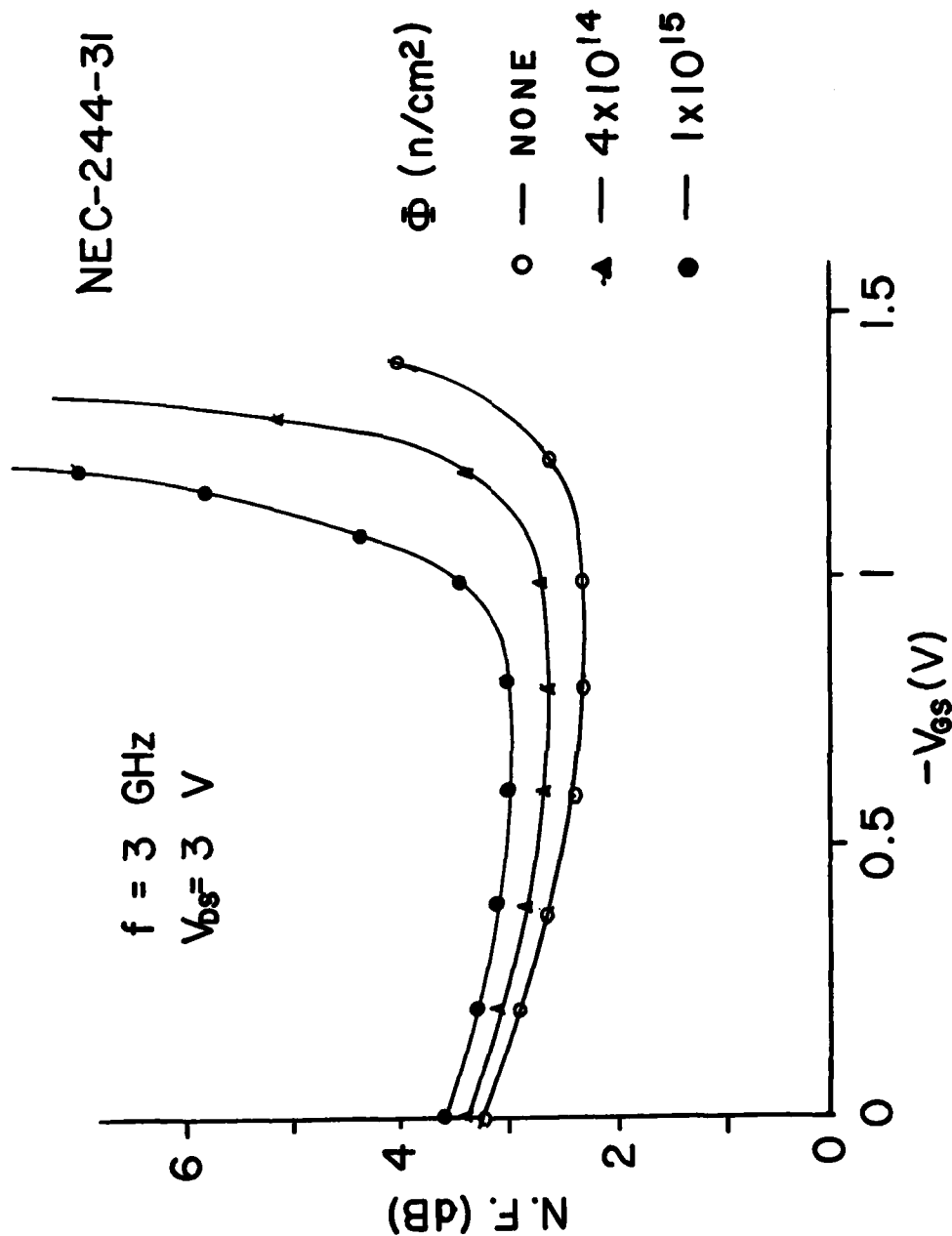


FIG. 3.12 - CHANGE IN THE NOISE FIGURE VS. GATE VOLTAGE CHARACTERISTICS AT 3 GHz AFTER HIGH NEUTRON FLUENCE.

GAT-5-48

$f = 3 \text{ GHz}$

$V_{DS} = 3 \text{ V}$

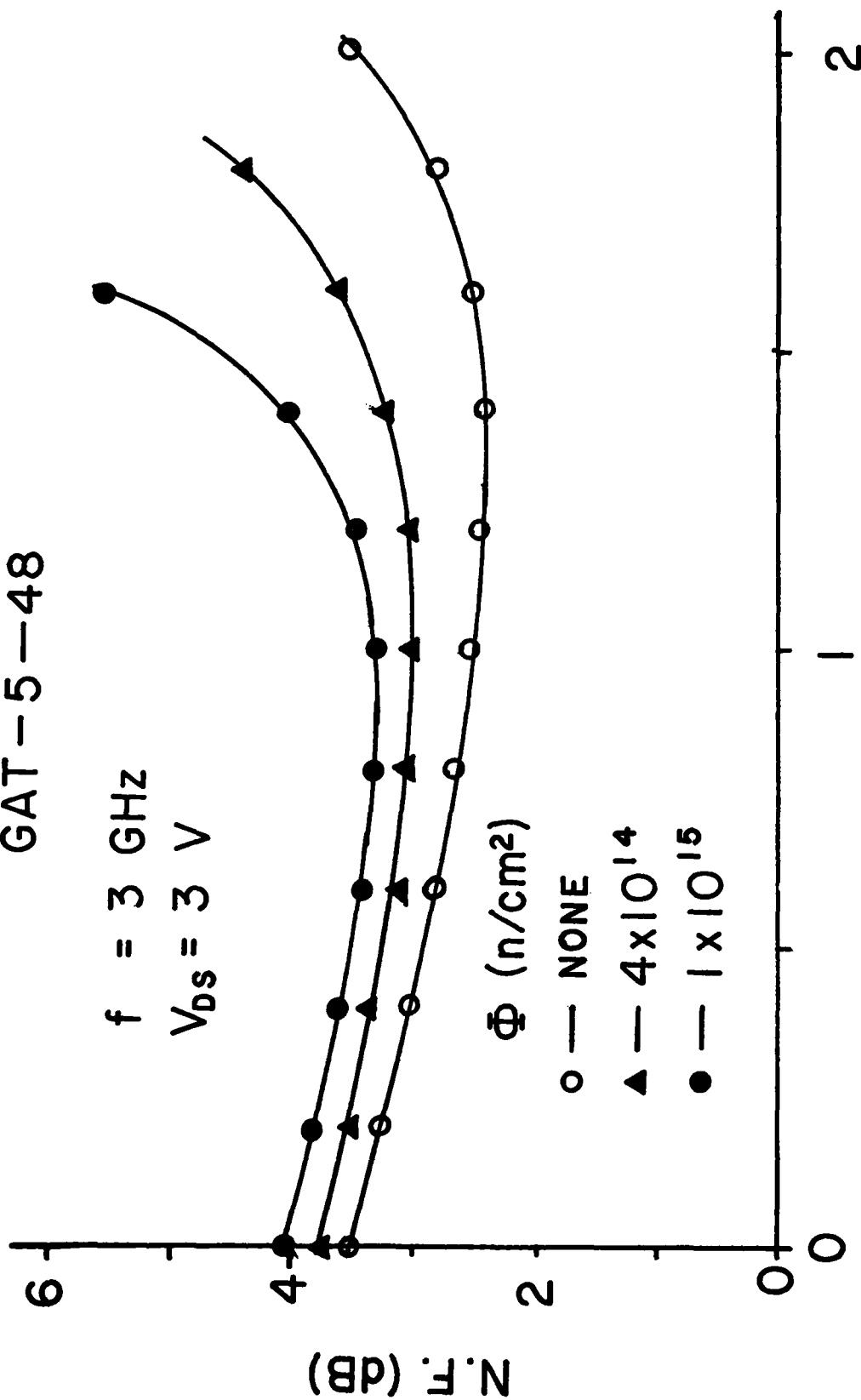


FIG. 3.13 - CHANGE IN THE NOISE FIGURE VS. GATE VOLTAGE CHARACTERISTICS AT 3 GHz AFTER HIGH NEUTRON FLUENCE.

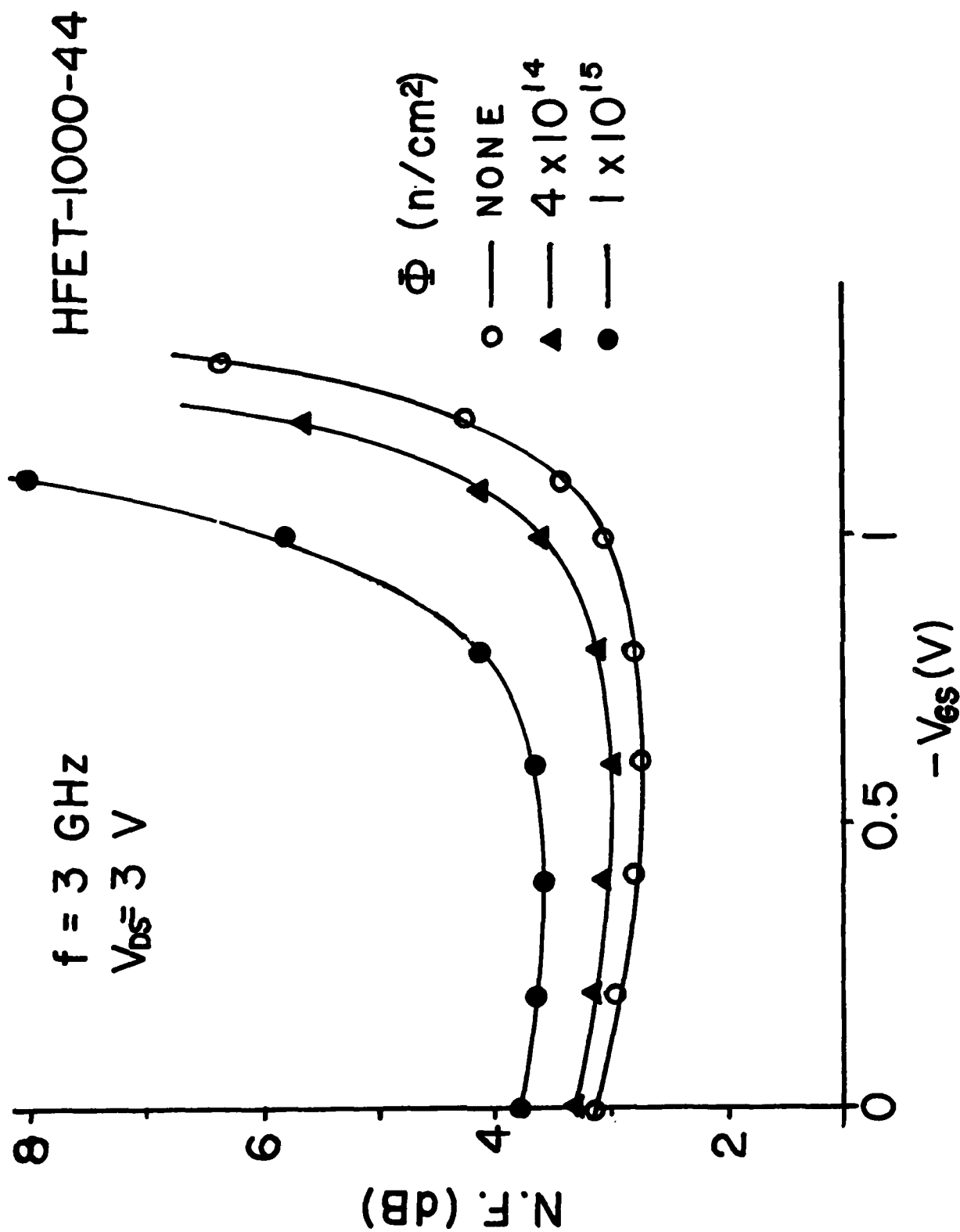


FIG. 3.14 - CHANGE IN THE NOISE FIGURE VS. GATE VOLTAGE CHARACTERISTICS AT 3 GHz AFTER HIGH NEUTRON FLUENCE

NEC-244-31

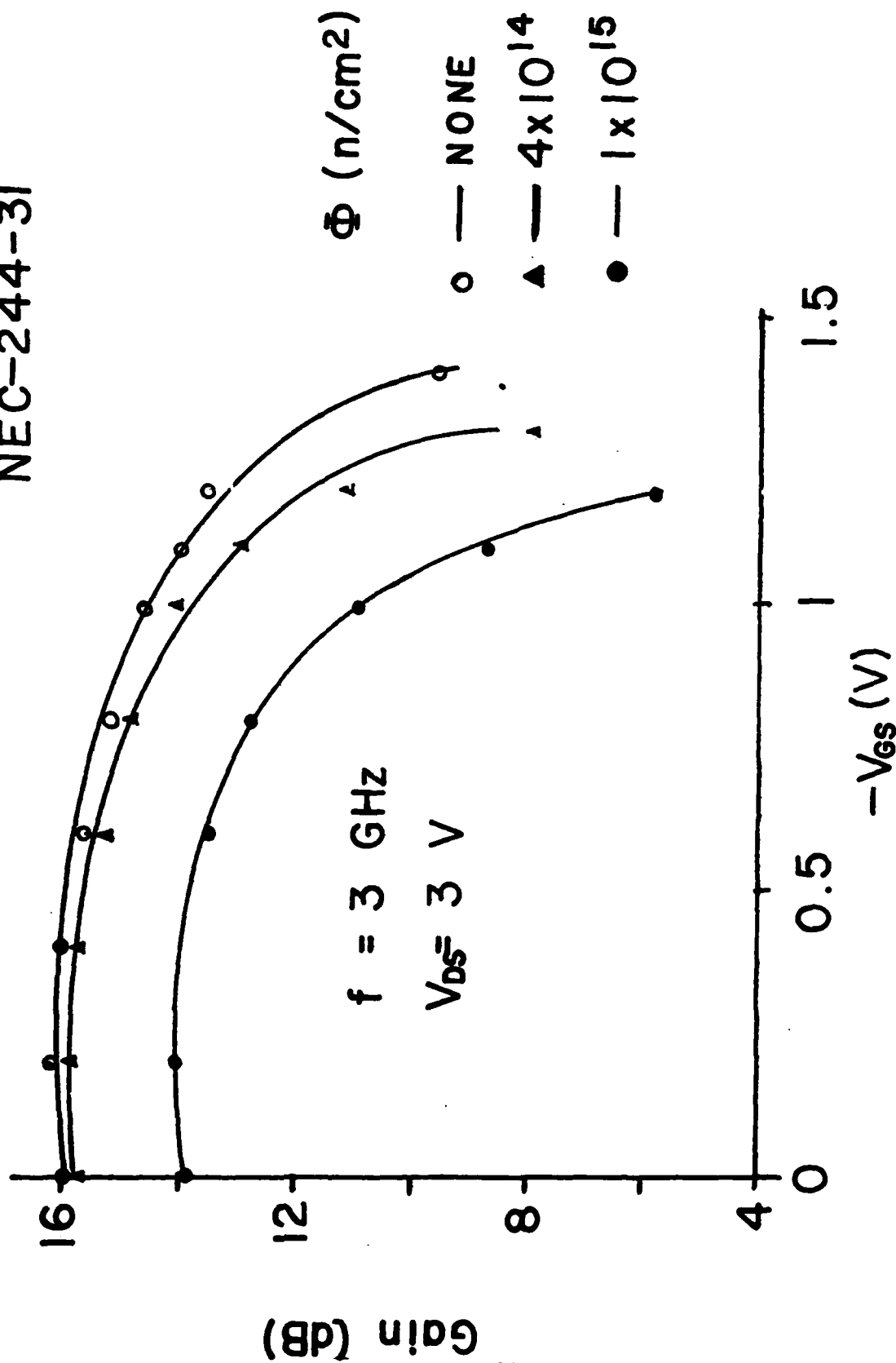


FIG. 3.15 - CHANGE IN THE AMPLIFIER GAIN VS. GATE VOLTAGE CHARACTERISTICS AT 3 GHz AFTER HIGH NEUTRON FLUENCE.



GAT-5-48

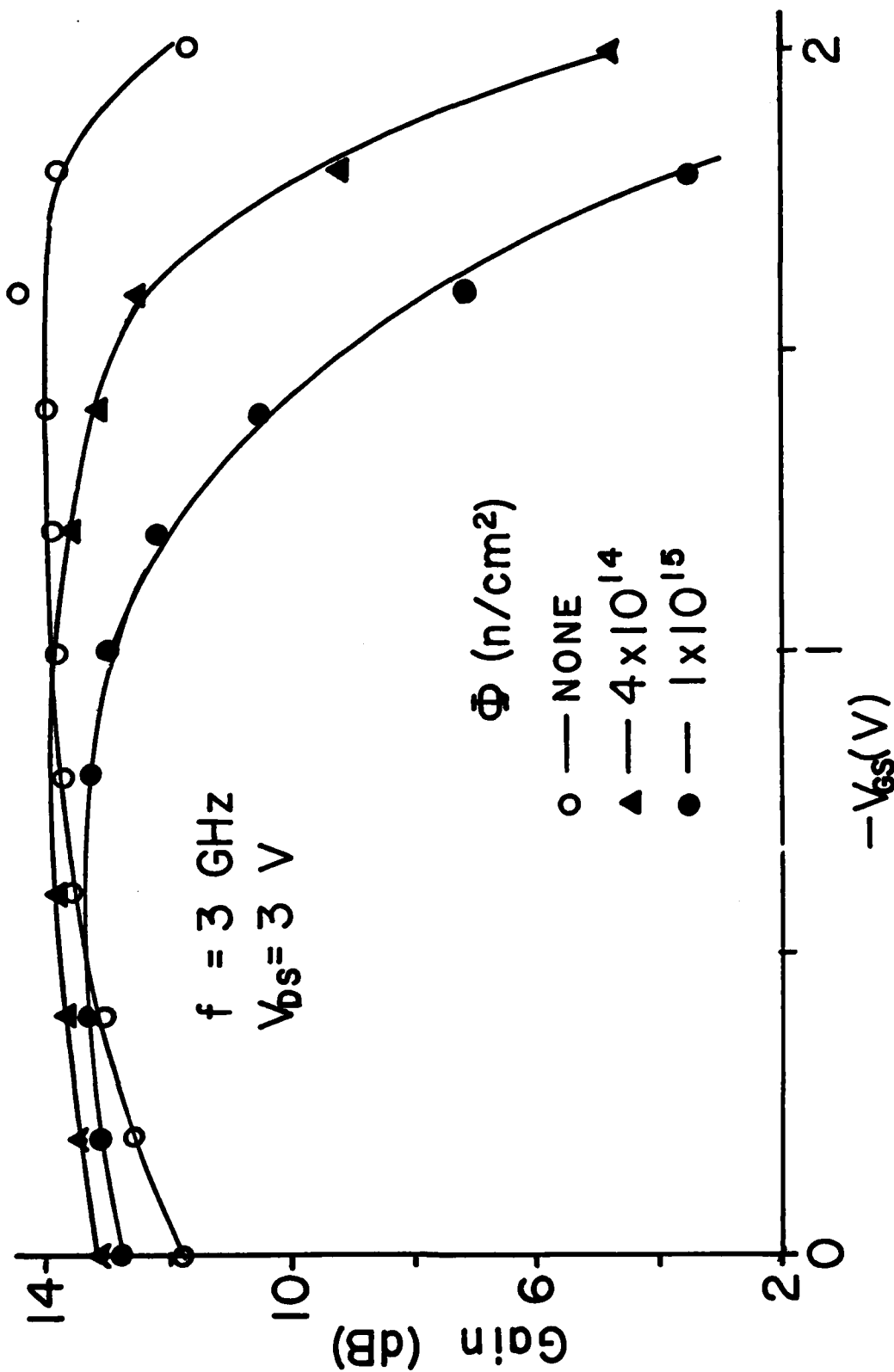


FIG. 3.16 - CHANGE IN THE AMPLIFIER GAIN VS. GATE VOLTAGE CHARACTERISTICS AT 3 GHz AFTER HIGH NEUTRON FLUENCE

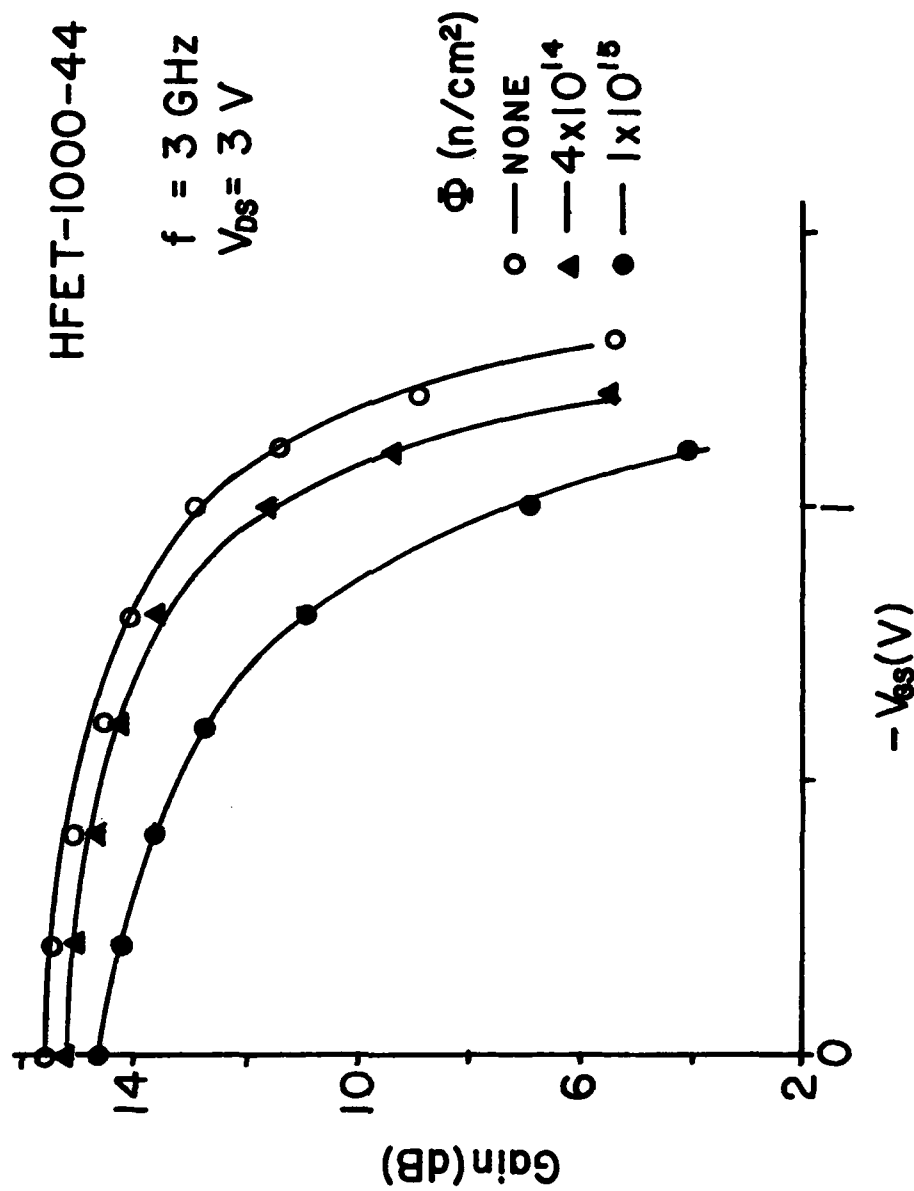


Fig. 3.17 - Change in the Amplifier Gain vs. Gate Voltage Characteristics at 3 GHz after High Neutron Fluence.

observed in the DC  $I_D$  vs.  $V_D$  characteristics discussed in Sec. 3.3. It should be pointed out that the increase in the minimum noise figure is of the order of 0.7 dB at  $1 \times 10^{15}$  n/cm<sup>2</sup>, however if the gate bias voltage remains the same as before irradiation then the increase in noise figure is of the order of 1.3 dB.

The degradation in the amplifier gain is appreciable at a fluence of  $1 \times 10^{15}$  n/cm<sup>2</sup>. Below this fluence the change is caused by the slight change in the transconductance and parasite series resistance. At a fluence of  $1 \times 10^{15}$  n/cm<sup>2</sup> there is a large change in the gain. This is caused by deterioration of the transconductance, increase of the parasitic series resistance and possibly a change in the reactive elements such as gate to source capacitance. At these fluences compensation starts to take place in the part of the active layer which is doped approximately to  $10^{17}$  per cm<sup>3</sup> since the neutron carrier removal in GaAs is of the order of  $10$  cm<sup>-1</sup>. The shape of the dependence of noise figure and amplifier gain with frequency was almost invariant with neutron fluence. As the neutron fluence was increased there was a monotonic deterioration of amplifier performance without changing its bandwidth except at the highest fluence.

Figs. 3.18 to 3.23 show the noise figure and transducer power gain for the same devices at X-band. At this frequency optimum tuning was not achieved in the HFET-1000-44 because the S-band discs were fixed. The noise figure at X-band is higher than at S-band because of its dependence upon frequency and the amplifier gain is lower because at these frequency parasitic elements such as source resistance, source inductance and gate to drain capacitance start to dominate the gain characteristics. At X-band frequencies, slight changes in any of these parameters affect the gain to

NEC-244-31

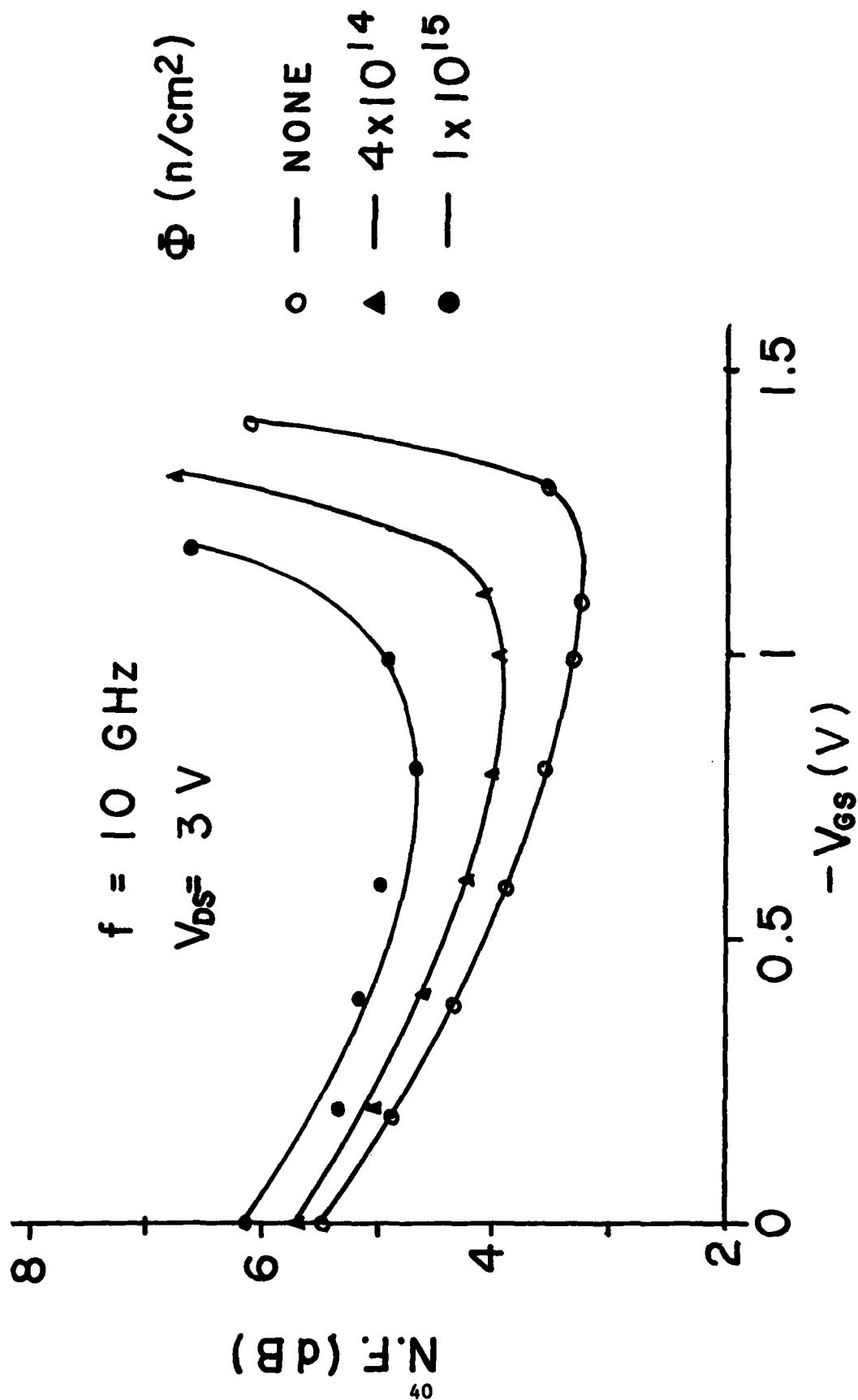


FIG. 3.18 - NOISE FIGURE VS. GATE VOLTAGE AT X-BAND AFTER HIGH NEUTRON FLUENCE.

GAT-5-48

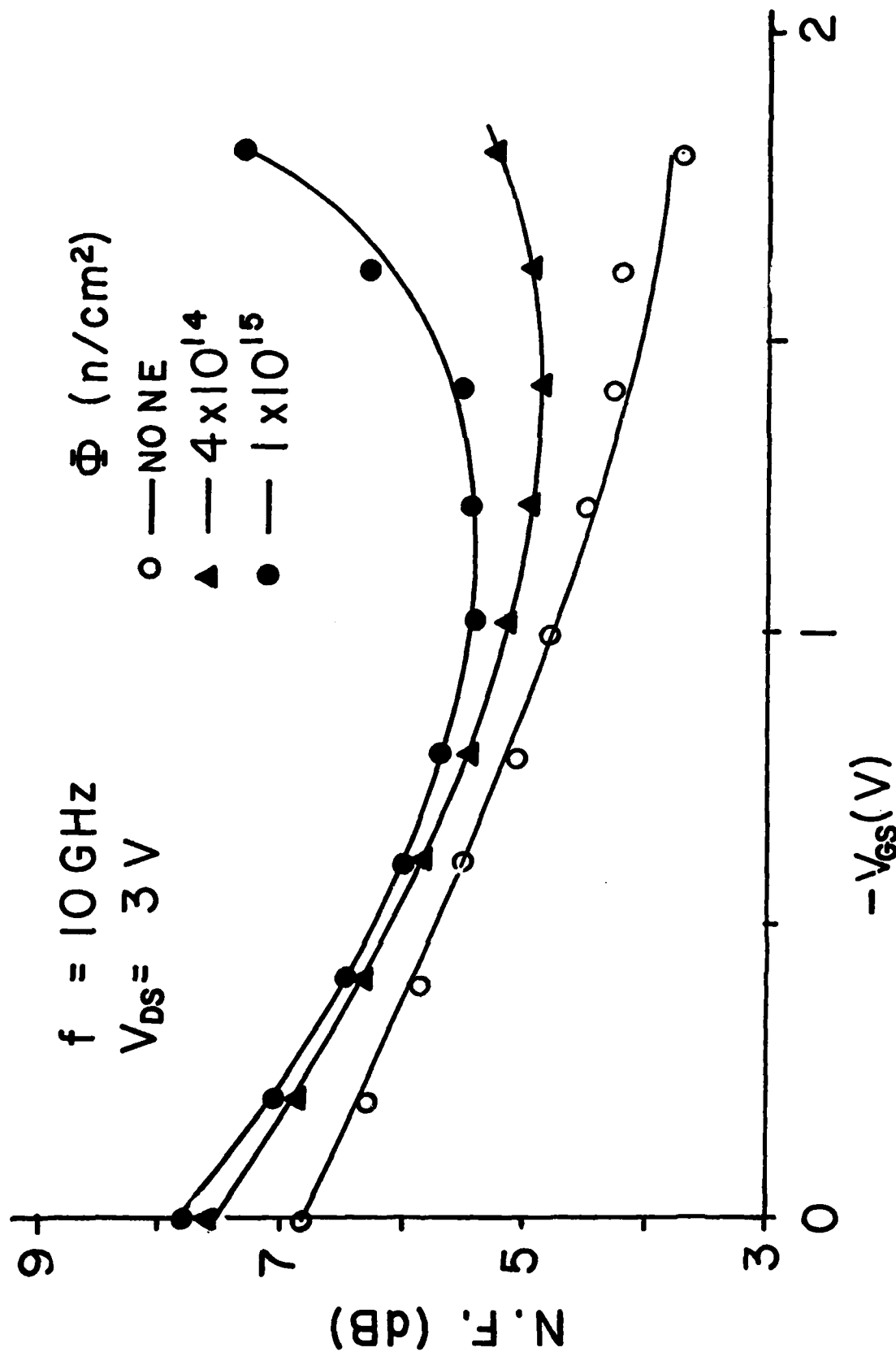


FIG. 3.19 - NOISE FIGURE VS. GATE VOLTAGE AT X-BAND AFTER HIGH NEUTRON FLUENCE

HFET-1000-44

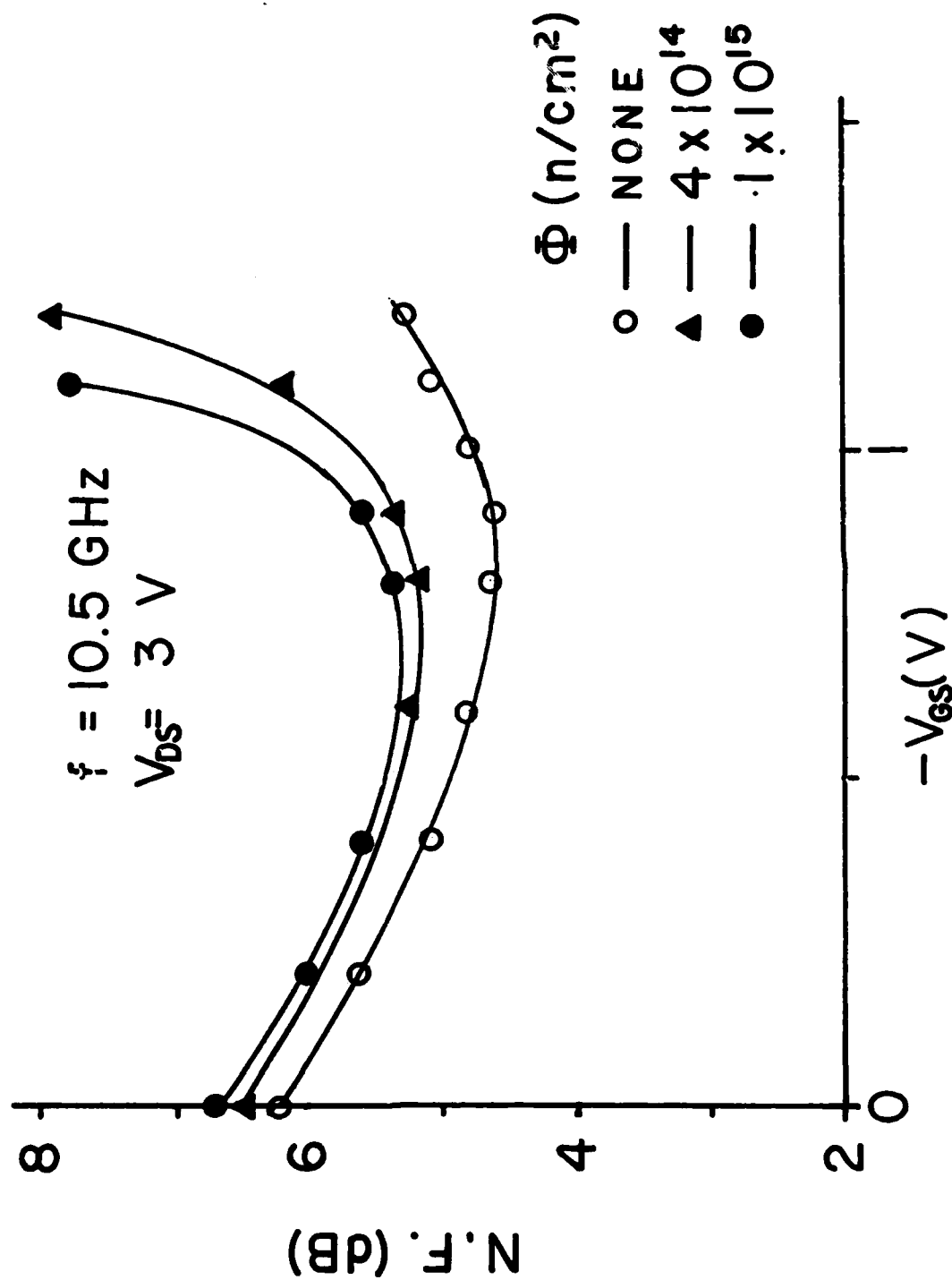


Fig. 3.20 - NOISE FIGURE VS. GATE VOLTAGE AT X-BAND AFTER HIGH NEUTRON FLUENCE.

NEC-244-31

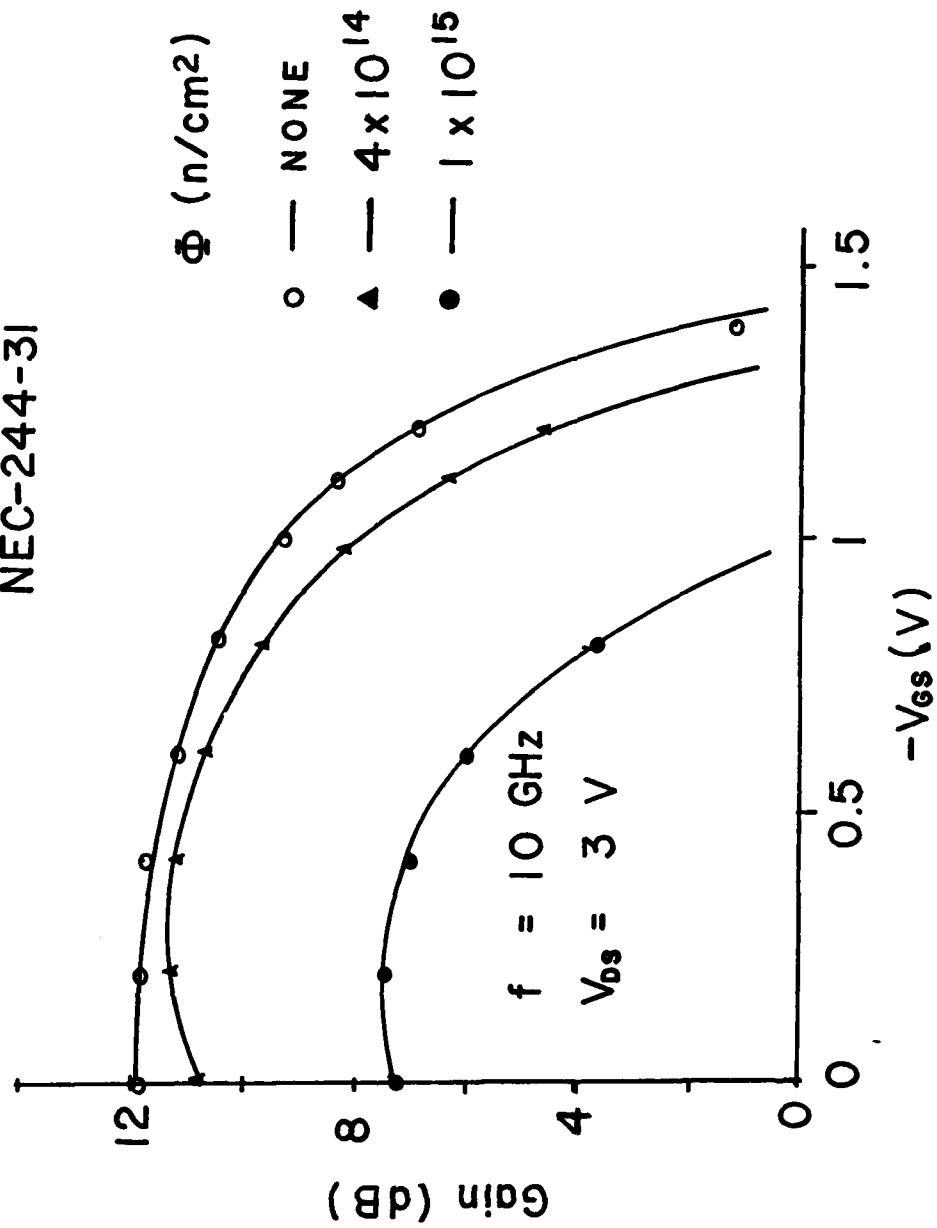


FIG. 3.21 - AMPLIFIER GAIN VS. GATE VOLTAGE AT X-BAND AFTER HIGH NEUTRON FLUENCE.

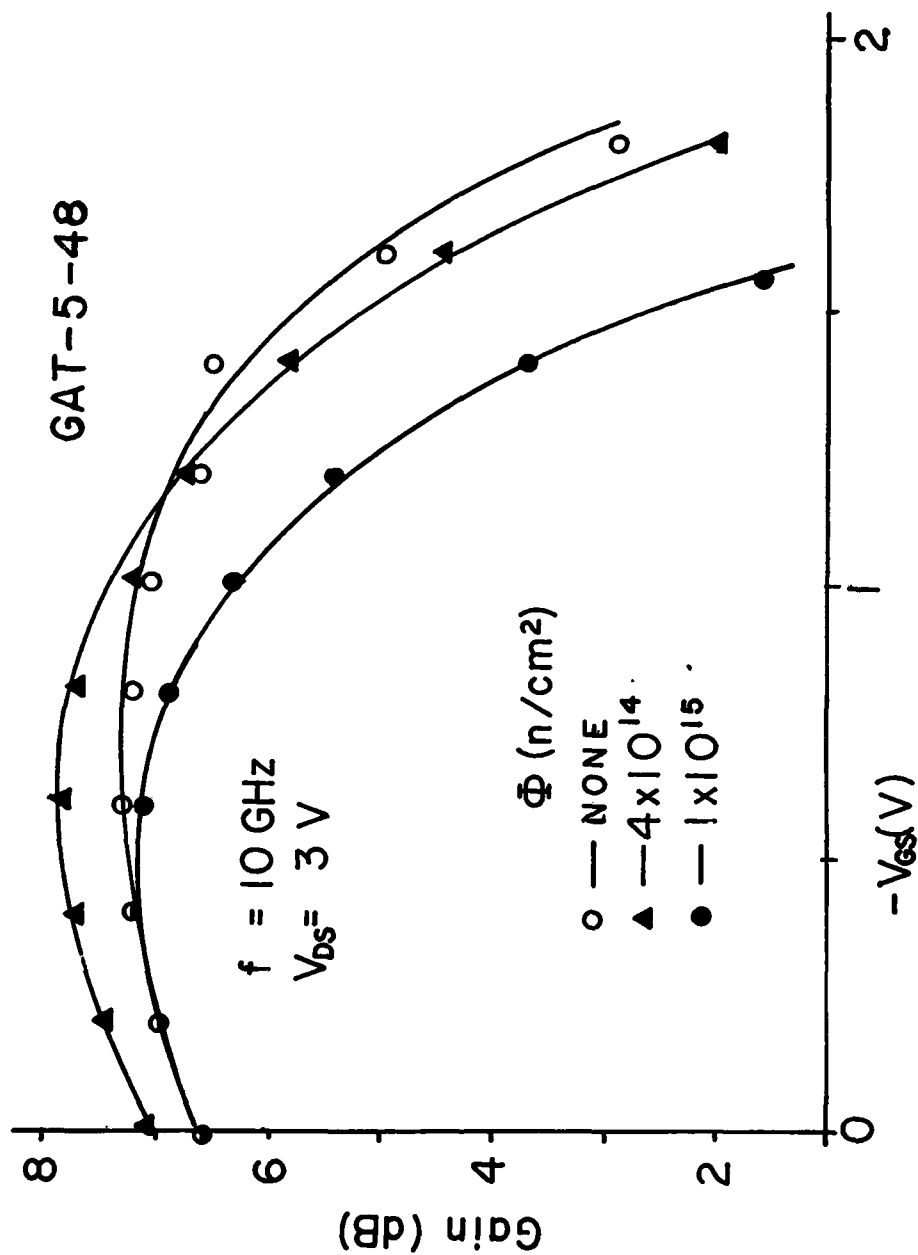


FIG. 3.22 - AMPLIFIER GAIN VS. GATE VOLTAGE AT X-BAND AFTER HIGH NEUTRON FLUENCE.



HFET-1000-44

$f = 10.5 \text{ GHz}$

$V_{DS} = 3 \text{ V}$

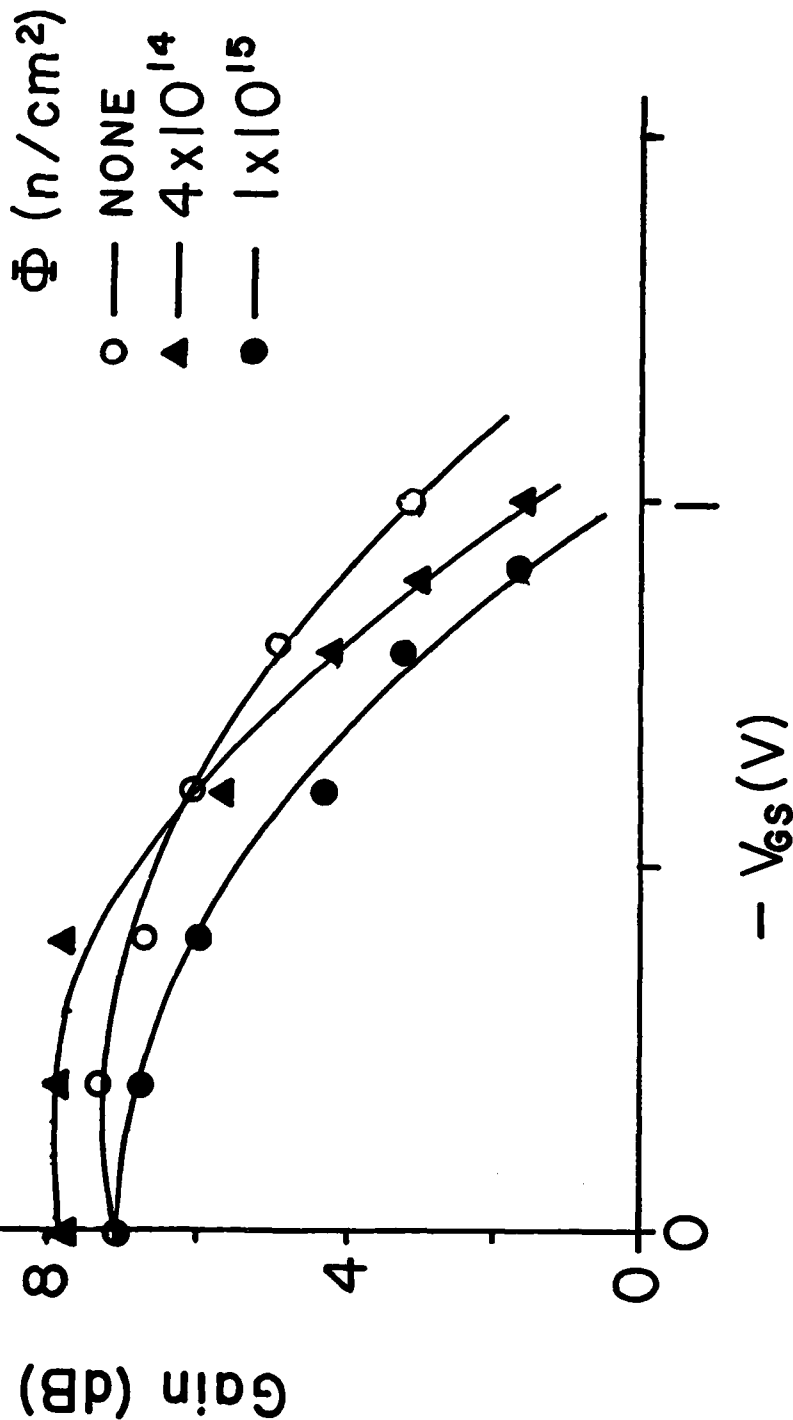


FIG. 3.23 - AMPLIFIER GAIN VS. GATE VOLTAGE AT X-BAND AFTER HIGH NEUTRON FLUENCE.

a larger extent than they do at S-band. We believe that the large deterioration that is observed on the gain at  $1 \times 10^{15} \text{ n/cm}^2$ , compared to the one observed at  $4 \times 10^{14} \text{ n/cm}^2$ , is because of changes in the gate to source and gate to drain capacitances. As mentioned previously, compensation should start to take place at this high fluence. A summary of the changes observed in these devices is presented in Table 3.1.

A theory for the noise of GaAs MESFETs has been developed by Pucel et.al.<sup>5</sup> taking into account diffusion noise of the electrons moving at saturated velocity from source to drain. In this theory the minimum noise figure  $F$  is given by:

$$F = 1 + \frac{\omega C_{gs}}{g_m} \sqrt{k_g (k_r + g_m r_s)} \quad (3.1)$$

where  $\omega$  is the frequency of operation,  $C_{gs}$  is the gate to source capacitance,  $g_m$  is the transconductance,  $r_s$  is any parasitic series resistance in the gate-source terminals and  $k_g$  and  $k_r$  are parameters related to noise correlation between drain and gate. For microwave FETs the value of  $k_r$  is an order of magnitude less than  $g_m r_s$ , except close to pinch-off, so that Eq. (3.1) can be simplified to:

$$F = 1 + \omega C_{gs} \sqrt{k_g r_s / g_m} \quad (3.2)$$

The value of  $k_g$  depends upon the device dimensions and upon the drain current but in the first approximation it can be considered gate bias voltage dependent. If that is the case, it is possible to relate the noise figure  $F_R$  after irradiation to the noise figure  $F_0$  before irradiation in terms of the values of  $g_m$  and  $r_s$  before and after irradiation at each gate bias voltage. That is from Eq. (3.2) it follows that:

Table 3.1 Amplifier Characteristics Before and After Neutron Irradiation  
with Pre-Irradiation Minimum Noise Figure Bias.

Device	Characteristic	S Band		X Band	
		Before Irradiation	$10^{15} \text{ n/cm}^2$	Before Irradiation	$10^{15} \text{ n/cm}^2$
NEC 244-31	Noise Figure (dB)	2.3	3.5	3.3	5.7
	Gain	14.5	11.0	9.1	<3.0 dB
HFET 1000-44	Noise Figure (dB)	2.7	4.1	4.6*	5.6
	Gain (dB)	14.0	11.0	4.5*	3.1
GAT 5-48	Noise Figure (dB)	2.4	3.8	4.2	5.8
	Gain (dB)	14.0	12.1	5.6	2.5

\* Optimum pre-irradiation tuning not possible with fixed S band disc.

$$\frac{F_R - 1}{F_o - 1} = \frac{(\sqrt{r_s/g_m})_R}{(\sqrt{r_s/g_m})_o} \quad (3.3)$$

assuming that the gate to source capacitance does not change with irradiation. This is not a bad assumption at fluences below  $10^{15}$  n/cm<sup>2</sup> where carrier removal is small compared to the background doping of the active layer. For fluences at and above  $10^{15}$  n/cm<sup>2</sup> that assumption may not be valid but any change in capacitance will be neglected. In order to check if Eq. (3.3) applies, we measured the source to drain resistance  $R_{ds}$  from the linear part of the  $I_D$  vs.  $V_D$  characteristics and plotted it as a function of normalized gate bias. The plot is shown in Fig. 3.24 for the NEC-244-31 and the extrapolation gives the value of the parasitic source to drain resistance  $r_s + r_d$  which can be split equally between source  $r_s$  and drain resistance  $r_d$ . We also measured the transconductance  $g_m$  at 1 MHz as a function of gate bias after irradiation and it is shown in Fig. 3.6. Using the results of Figs. 3.6 and 3.24 and the noise figure measured before irradiation, we have calculated the noise figure using Eq. (3.3) and the results for the NEC device are shown in Fig. 3.25. There is good agreement between theory and experiment except close to pinch-off, indicating that the degradation in microwave noise of the GaAs MESFET due to neutron radiation is caused by a decrease in the transconductance and an increase in the parasitic source resistance. Similar calculations were carried out for GAT-5-48 and HFET-1000-44 and the results are shown in Figs. 3.26 and 3.27. The agreement for these devices is not as good as the one obtained for the NEC-244-31.

Close to pinch-off the noise figure increases faster with gate bias than the one predicted by Eq. 3.3. We believe this is because close to pinch-off the term  $g_m r_s$  is smaller than  $k_r$  in Eq. (3.1). If this is the

NEC-244-31

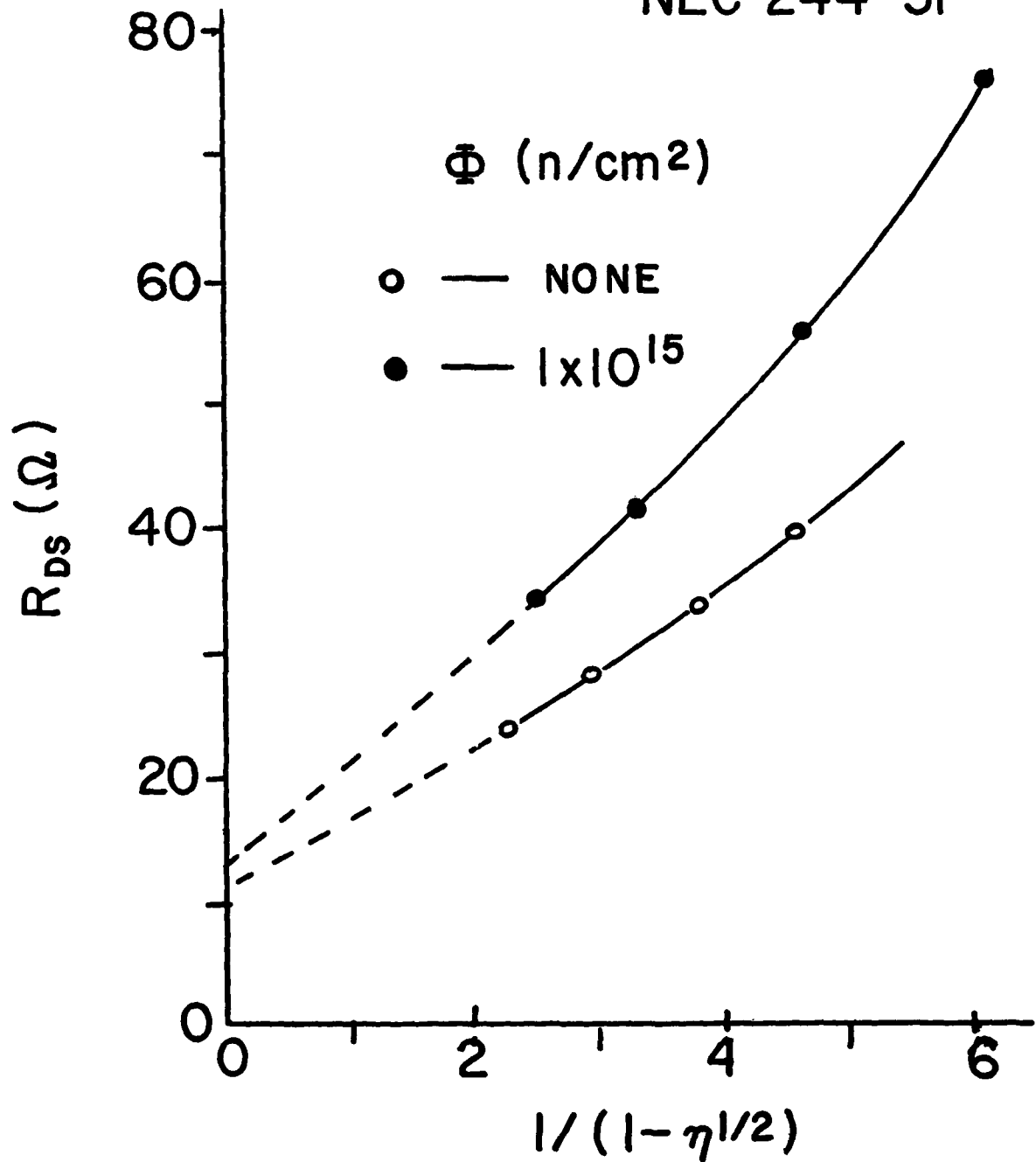


FIG. 3.24 - DRAIN TO SOURCE RESISTANCE AS A FUNCTION OF NORMALIZED GATE VOLTAGE.

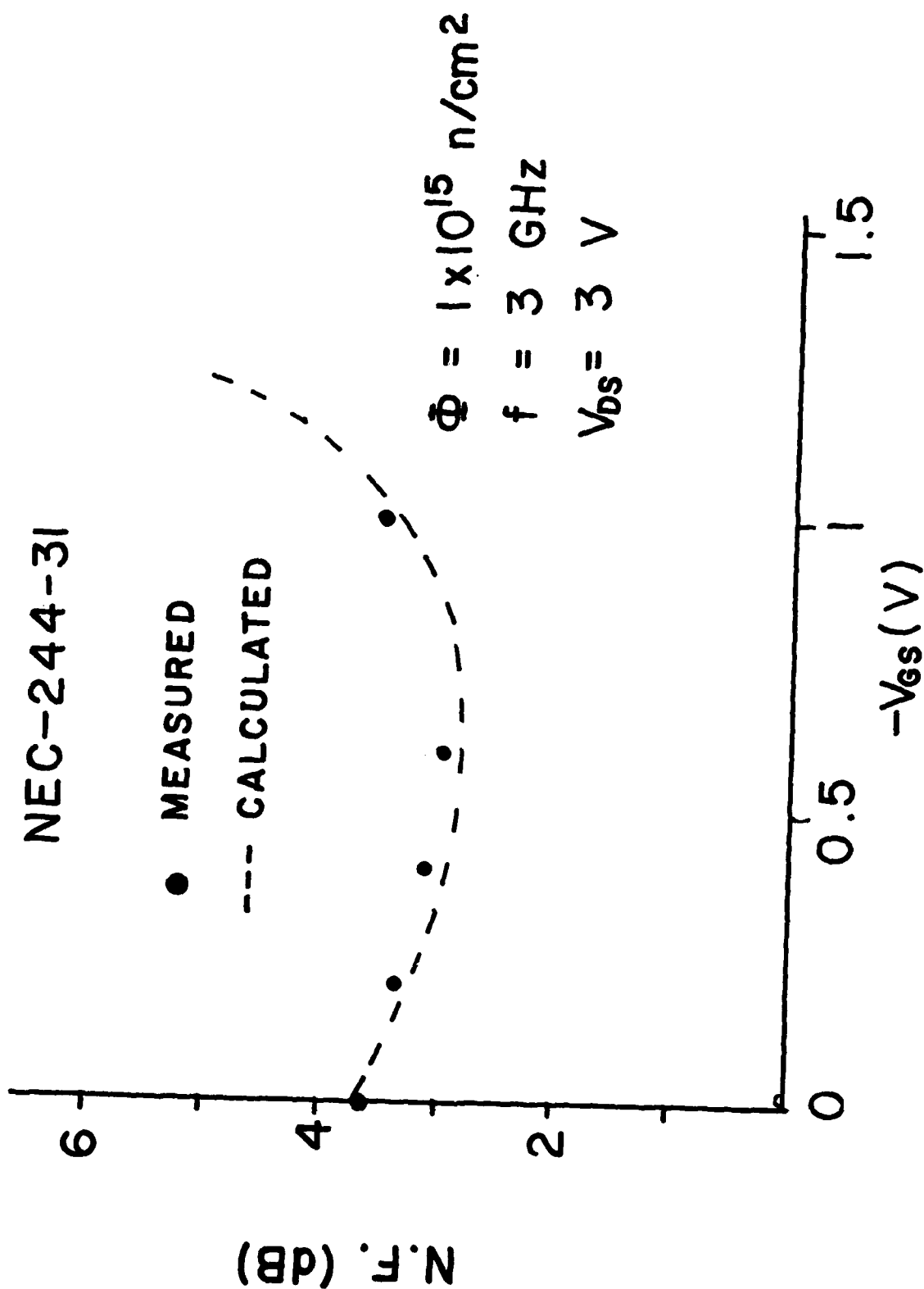


FIG. 3.25 - MEASURED AND PREDICTED NOISE FIGURE VS. GATE VOLTAGE AFTER  $1 \times 10^{15} \text{ N/CM}^2$ .

case, then Eq. (3.1) changes to:

$$F = 1 + \frac{\omega C}{g_m} \frac{g_s}{\sqrt{k_g k_r}} \quad (3.4)$$

Using the above equation instead to Eq. (3.2), we can relate the noise figures before and after irradiation and we obtain:

$$\frac{F_R - 1}{F_O - 1} = \frac{(g_m)_O}{(g_m)_R} \quad (3.5)$$

which has a stronger dependence upon  $g_m$  than Eq. (3.3) does. We have used the above equation for gate voltages close to pinch-off and plotted the calculated results in Figs. 3.26 and 3.27 for devices GAT-5-48 and HFET-1000-44. The figures show that indeed the increase in noise figure close to pinch-off is better described by Eq. (3.5) than by Eq. (3.3).

The above results indicate that the degradation in microwave noise due to neutron irradiation in GaAs MESFETs is due mainly to a decrease in the transconductance and an increase in the parasitic series resistance. For gate voltages close to zero bias the degradation appears to follow Eq. (3.3) and close to pinch-off follows Eq. (3.5). Although at the neutron fluences tested the amount of traps introduced is appreciable as indicated by low frequency noise measurements, these traps do not seem to affect the microwave noise.

### 3.5 $\gamma$ -Radiation Results:

Figs. 3.28 and 3.29 show the noise figure and transducer power gain at 3 and 9 GHz respectively for a Plessey GAT-5 device before and after  $2 \times 10^7$  rads (Si). This amplifier was optimally tuned for minimum noise figure at 3 GHz and the discs epoxied to the microstrip. The noise figure before  $\gamma$ -irradiation appears to be slightly high because it was taken after the device had been irradiated to  $1 \times 10^{13}$  n/cm<sup>2</sup>. The data shows that the gain is

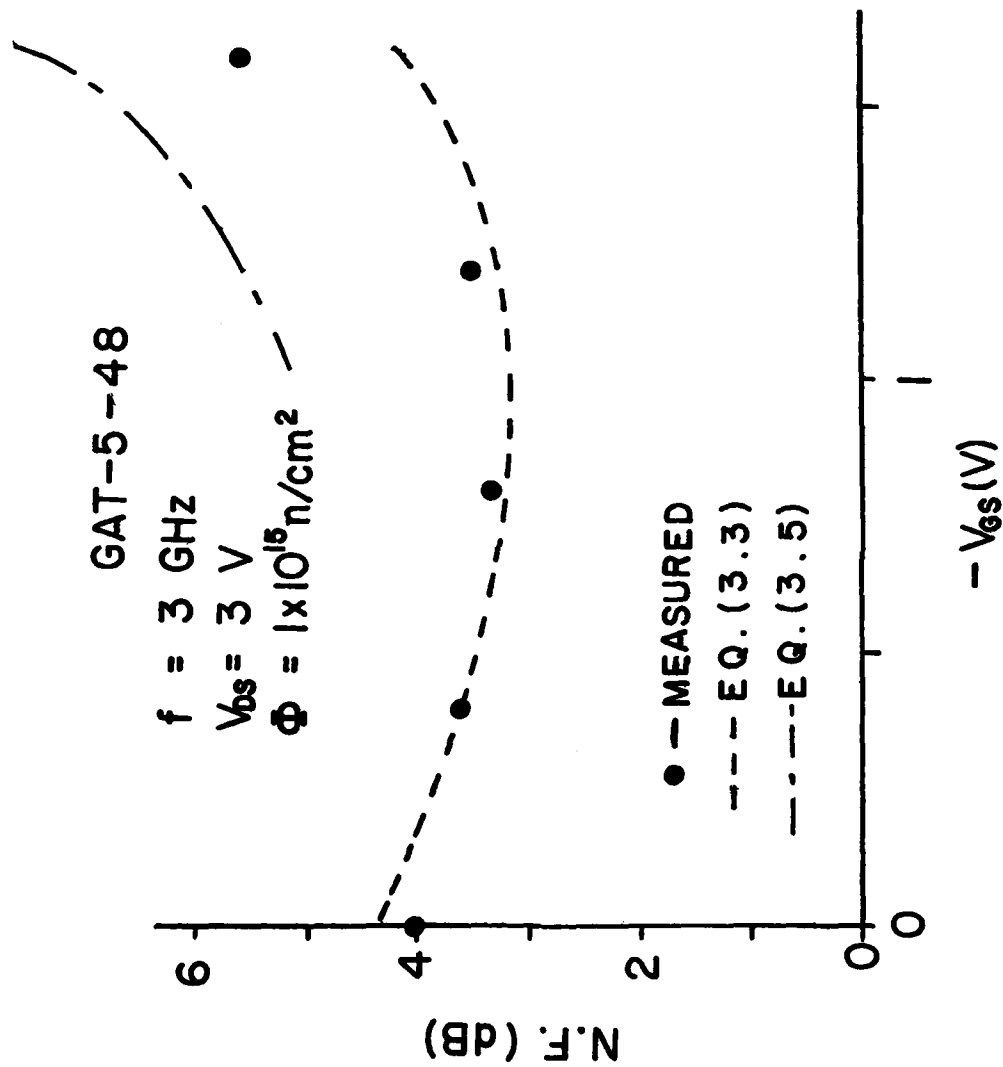


FIG. 3.26 - MEASURED AND PREDICTED NOISE FIGURE VS. GATE VOLTAGE AFTER  $1 \times 10^{15} \text{ n/cm}^2$ .



HFET-1000-44

$f = 3 \text{ GHz}$

$V_{DS} = 3 \text{ V}$

$\Phi = 1 \times 10^{15} \text{ n/cm}^2$

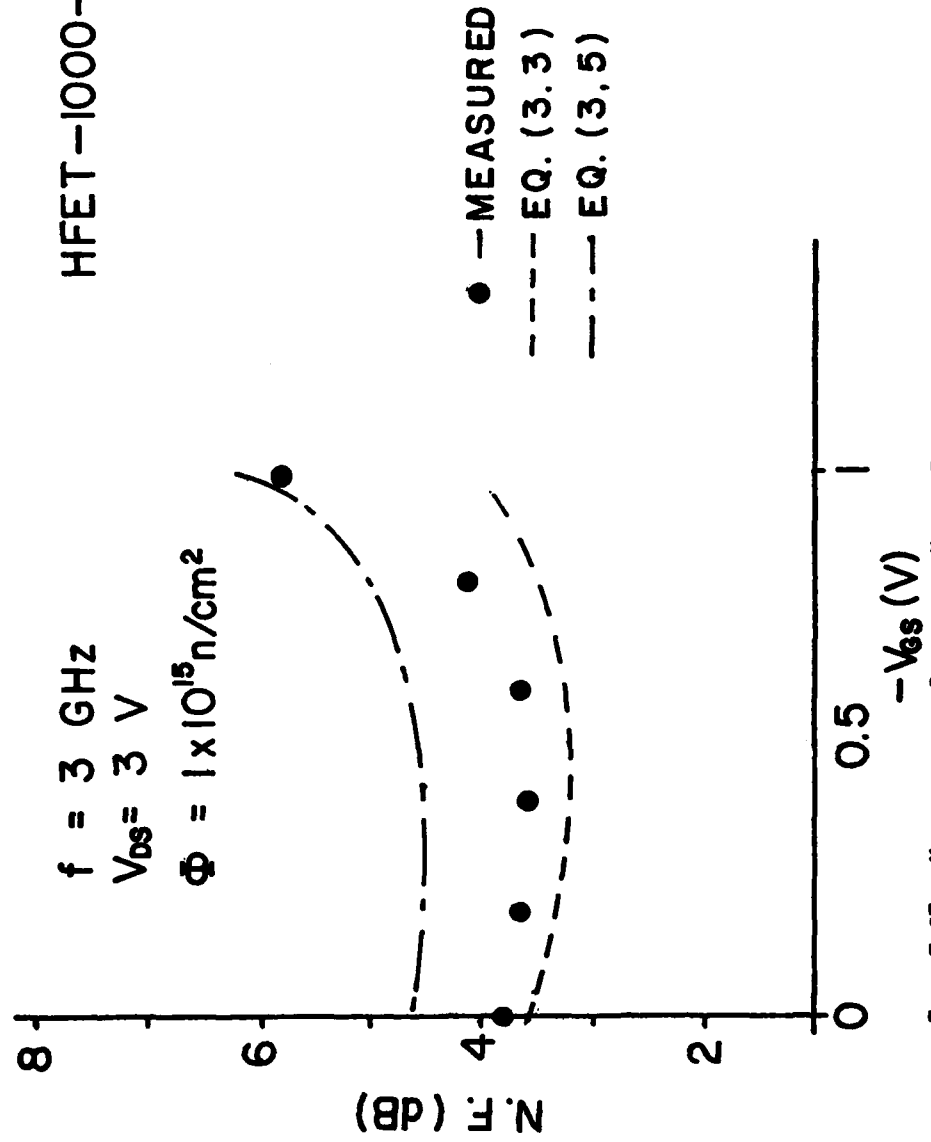


FIG. 3.27 - MEASURED AND PREDICTED NOISE FIGURE VS. GATE VOLTAGE AFTER  $1 \times 10^{15} \text{ n/cm}^2$ .

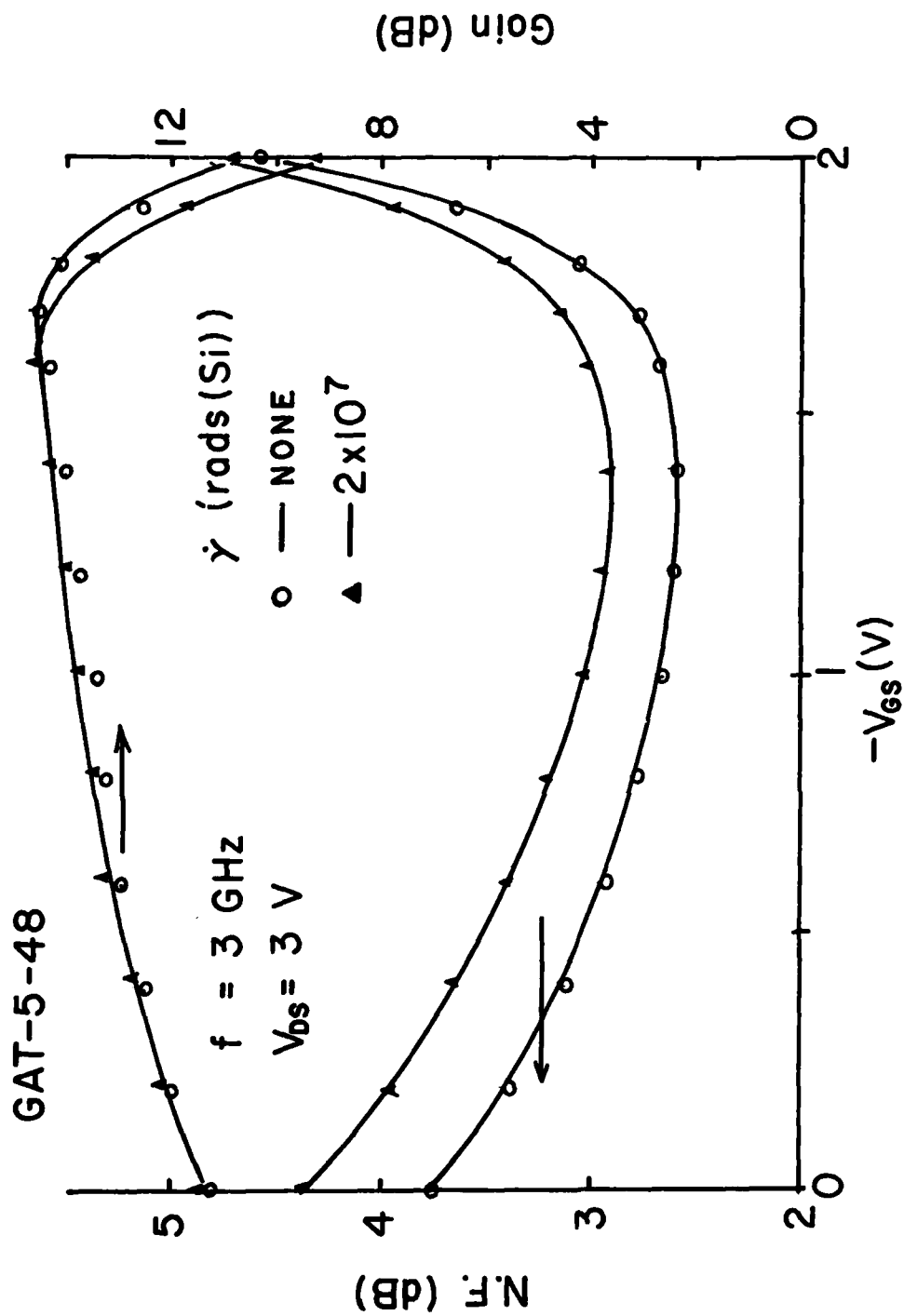


FIG. 3.28 -  $\gamma$ -IRRADIATED AMPLIFIER CHARACTERISTICS VS. GATE VOLTAGE AT 3 GHz.

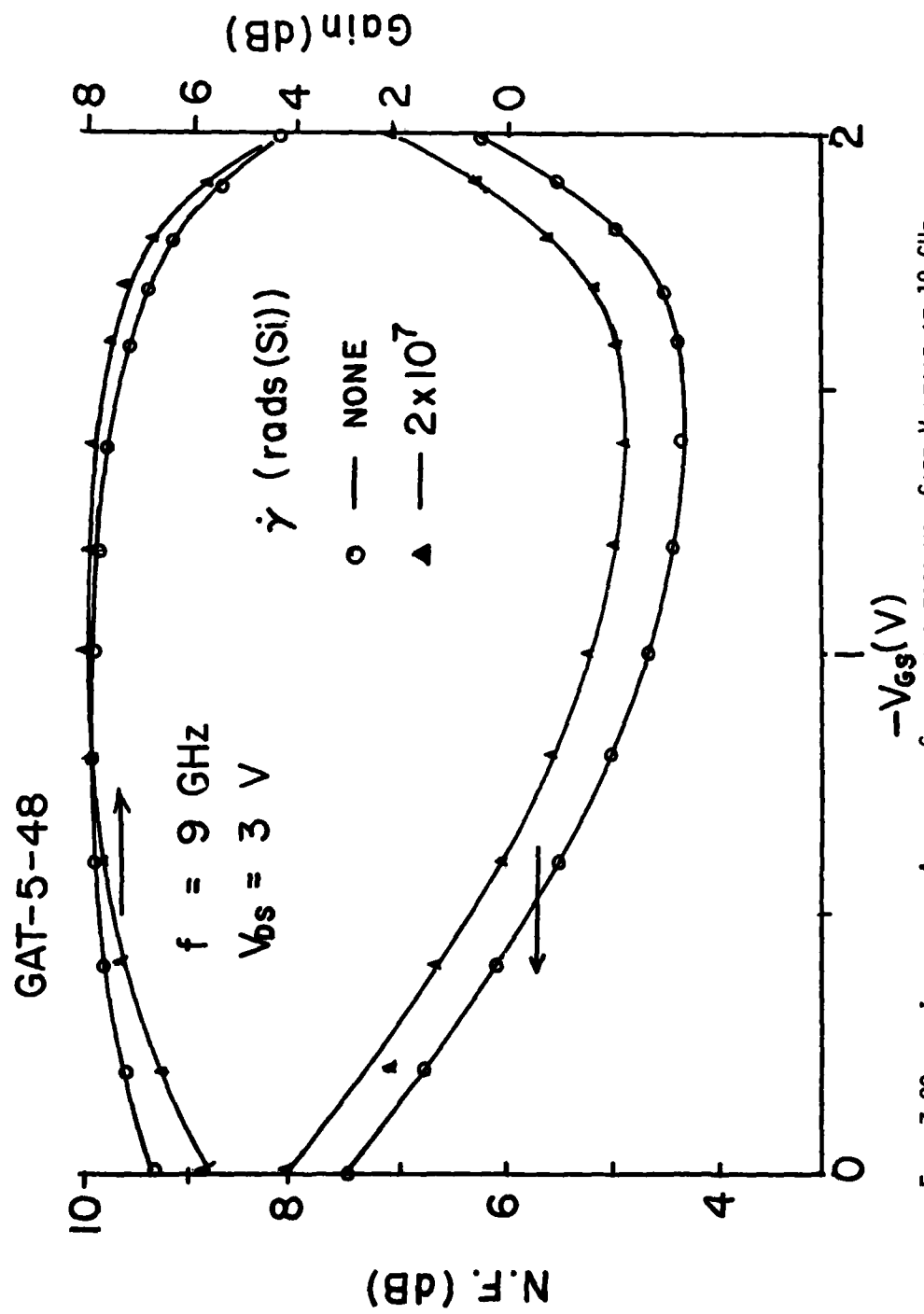


Fig. 3.29 -  $\gamma$ -IRRADIATED AMPLIFIER CHARACTERISTICS VS. GATE VOLTAGE AT 10 GHz.

unaffected by  $\gamma$ -irradiation up to that dose but the noise figure increased by 0.4 dB at 3 GHz and by 0.6 dB at 9 GHz. This increase in noise figure takes place before there is any appreciable change in the small signal parameters of the device as determined from microwave measurements and by 1 MHz small signal parameters measurements. At that dose the DC characteristics and the small signal parameters change less than 5% from their pre-irradiation value.

The increase in noise figure in this case cannot be explained in the same way as it was explained for the neutron radiation case. The increase in noise figure may be caused by traps due to radiation damage. This is quite possible since at dose levels of  $2 \times 10^7$  rads (Si),  $\gamma$ -radiation must certainly produce displacement damage. In order to check for any additional traps, the low frequency noise was measured before and after  $\gamma$ -irradiation. No appreciable change was observed as it was found in the case of neutron radiation. We can only conclude that the concentration of traps introduced by  $\gamma$ -irradiation which affect low frequency noise must be less than the concentration present before irradiation.

#### 4. CONCLUSIONS

In this program we evaluated the change in microwave noise and gain of GaAs MESFET S- and X-band amplifiers with neutron and  $\gamma$ -radiation. Source amplifiers were realized in alumina microstrip using commercial devices from Nippon Electric, Plessey and Hewlett-Packard. The amplifiers were exposed to neutron radiation with two different radiation sources. One of them was the Van der Graaf accelerator at Hanscom AFB which produced a 5.5 MeV monoenergetic neutron beam. With this neutron source no degradation was observed in the microwave characteristics of the amplifiers up to the maximum fluence used of  $4.5 \times 10^{13}$  n/cm<sup>2</sup>. The other neutron source was the water moderated BMR reactor at Brookhaven National Laboratory. A slight degradation in the noise figure at  $1 \times 10^{14}$  n/cm<sup>2</sup> and a large degradation of noise figure and amplifier gain at  $1 \times 10^{15}$  n/cm<sup>2</sup> were observed with this neutron source.

The degradation in noise figure was correlated to the decrease in transconductance  $g_m$  and increase in source resistance  $r_s$ . For gate bias voltages close to zero, the noise figure appears to degrade as  $\sqrt{r_s/g_m}$  for gate bias voltages close to pinch-off as  $1/g_m$ . The degradation in amplifier gain was caused not only by the decrease in  $g_m$  and increase but also by a change in the gate to source and gate to drain capacitance. This takes place at fluences of  $1 \times 10^{15}$  n/cm<sup>2</sup> when carrier removal starts to change that part of the active layer which is heavily doped ( $\approx 10^{17}$  cm<sup>-3</sup>). No correlation was found between the changes in low frequency noise (1 to 1.5 MHz) with the changes in noise figure.

Gamma-irradiation was found to increase the noise figure at a dose of  $2 \times 10^7$  rads (Si) without changing the signal characteristics of the device or the low frequency noise. This indicates that the change in microwave

could be due to additional traps introduced by  $\gamma$ -radiation and which respond to microwave frequencies. Since the low frequency noise was not affected, the trap concentration introduced appears to be less than the relevant trap concentration already present before irradiation.

## 5. BIBLIOGRAPHY

1. J. M. Borrego et.al., IEEE Trans. on Nuclear Science NS-25, 1436, (1978).
2. N. A. Slaymaker et.al., IEEE Trans. on Microwave Theory and Technique MTT-24, 329, (1976).
3. H. E. G. Luxton, Proc. 4th European Microwave Conference (Montreaux 1974), pp. 92-96.
4. S. B. Moghe et.al., Electronics Letters 14, 637, (1978).
5. R. A. Pucel et.al., Adv. in Electronic and Electron Physics 38, New York Academic Press, 1975, pp. 195-265.



## MISSION of *Rome Air Development Center*

RADC plans and executes research, development, test and selected acquisition programs in support of Command, Control Communications and Intelligence (C<sup>3</sup>I) activities. Technical and engineering support within areas of technical competence is provided to ESD Program Offices (POs) and other ESD elements. The principal technical mission areas are communications, electromagnetic guidance and control, surveillance of ground and aerospace objects, intelligence data collection and handling, information system technology, ionospheric propagation, solid state sciences, microwave physics and electronic reliability, maintainability and compatibility.